Materials Advances

ROYAL SOCIETY OF CHEMISTRY

REVIEW

View Article Online
View Journal | View Issue

Check for updates

Cite this: *Mater. Adv.*, 2026, 7, 5458

Computer-aided hydrogel synthesis for 3D bioprinting: application of design of experiments (DoE), machine learning (ML), and computational fluid dynamics (CFD)

Minh Hien Nguyen, *[ab] Gia Huy Duong, [c] Le Thao Vy Huynh, [c] Hoang Cac Tien Le, [c] Thi Yen Nhi Nguyen, [ab] Vinh-Dat Vuong [bc] and Thi Tan Pham *[bc]

The hydrophilic polymeric network of hydrogels is a crucial element of bioinks, closely resembling the extracellular matrix and offering a supportive microenvironment vital for sustaining cell viability. Crucial rheological properties, especially viscosity and shear-thinning characteristics, are essential in influencing the printability and structural integrity of bioprinted constructs. Additionally, hydrogels must demonstrate suitable mechanical properties to support three-dimensional structures after printing and promote cellular proliferation and differentiation. This review highlights the incorporation of advanced methodologies such as design of experiments (DoE), machine learning (ML), and computational fluid dynamics (CFD) in the systematic optimization of hydrogel formulations for 3D bioprinting applications. For example, DoE, specifically response surface methodology, has been utilized to optimize the concentrations of essential components, such as gelatin, alginate, and methylcellulose, resulting in excellent extrusion rheological characteristics. Simultaneously, machine learning techniques are progressively employed to model and automate the optimization process, diminishing dependence on trial-and-error experimentation and expediting bioink development. This review emphasizes the importance of a balanced strategy for improving the rheological and mechanical properties of hydrogels, which may be effectively realized through the combined use of DoE, ML and CFD approaches in 3D bioprinting.

Received 25th February 2026,
Accepted 29th April 2026

DOI: 10.1039/d6ma00268d

rsc.li/materials-advances

[a] *University of Health Sciences, Vietnam National University HCMC, Dong Hoa Ward, Ho Chi Minh City, Vietnam. E-mail: nmhien@uhsvnu.edu.vn*
[b] *Vietnam National University Ho Chi Minh City, Linh Xuan Ward, Ho Chi Minh City, Vietnam*
[c] *Ho Chi Minh City University of Technology (HCMUT), 268 Ly Thuong Kiet, Dien Hong Ward, Ho Chi Minh City, Vietnam. E-mail: ptthi@hcmut.edu.vn*

Minh Hien Nguyen

Associate Professor Minh Hien Nguyen received her PhD in Chemistry from Osaka University in 2016. She is currently the Vice Head of the Department of Medicinal and Organic Chemistry, Faculty of Pharmacy, University of Health Sciences, VNU-HCM. Her research bridges medicinal chemistry, natural products, drug delivery, and biomedical materials. Her recent studies integrate response surface methodology, in vitro and in silico assays, niosome-based delivery, and hydrogel platforms for 3D bioink development, with an emphasis on translating bioactive materials into pharmaceutical and biomedical applications.

Gia Huy Duong

Gia Huy Duong is a biomaterials researcher. He received his BEng in Engineering Physics from Ho Chi Minh City University of Technology, Vietnam National University-Ho Chi Minh City. His academic and professional background lies in applied physics and biomedical engineering, with research interests focused on advanced biomaterials and the application of machine learning to optimize biomanufacturing processes.

Open Access Article. Published on 29 April 2026. Downloaded on 6/12/2026 9:42:13 PM.
This article is licensed under a Creative Commons Attribution-NonCommercial 3.0 Unported Licence.

© 2026 The Author(s). Published by the Royal Society of Chemistry

Open Access Article. Published on 29 April 2026. Downloaded on 6/12/2026 9:42:13 PM. This article is licensed under a Creative Commons Attribution-NonCommercial 3.0 Unported Licence.

1. Introduction

Fused deposition modelling (FDM), developed from stereolithography in 1983 and patented in 1989,[1,2] is a form of 3D printing that can fabricate complex geometries at low cost with straightforward operational requirements. Due to its advantages, FDM has been widely used across aerospace, medical, and automotive sectors.[3–5] 3D bioprinting is a technique that integrates additive manufacturing and biomaterial deposition and has emerged as a powerful platform for the spatially controlled fabrication of biological constructs.[6,7] These days, 3D bioprinting expands its relevance in regenerative medicine, tissue engineering,[8,9] drug delivery,[10,11] and the development of implantable or organ replacements.[12]

Despite the significant promise in the biomedical field, the widespread application of 3D bioprinting remains constrained by several critical challenges. Chief among these are the difficulties in achieving high-resolution cell deposition, controlling cell distribution, or selecting the ideal bioink.[13] An ideal bioink must exhibit appropriate physicochemical characteristics,[14] including biocompatibility,[15,16] suitable rheology,[17] and mechanical properties, to support and preserve cellular viability and function throughout the printing process.[18] Furthermore, achieving high printing accuracy and speed requires high resolution, which requires selecting the appropriate printing technique and a suitable bioink formulation.[19]

A major limitation in 3D bioprinting for tissue engineering lies in the scarcity of bioinks.[20] The bioinks currently in use are based on natural and synthetic polymers.[21] While most natural polymers are cell-interacting and biocompatible,[22] they frequently lack the mechanical properties needed to maintain structural integrity and withstand physical stresses *in vivo*. To address these deficiencies, hydrogels have emerged as promising candidates due to their tuneable viscoelastic properties, high water content, and ability to support printability and cellular function. Their porous networks facilitate diffusion of oxygen and nutrients, enhance cellular mobility, and promote adhesion and proliferation within the extracellular matrix.[23,24] However, to achieve efficient hydrogel use in 3D bioprinting, it is necessary to accurately determine the

Le Thao Vy Huynh

Le Thao Vy Huynh is a Master of Engineering student at Ho Chi Minh City University of Technology, Vietnam National University-Ho Chi Minh City. She received her BEng in Engineering Physics from the same institution. Her academic background lies in applied physics and engineering, with research interests spanning materials science and its emerging applications in biomedical and technological fields.

Hoang Cac Tien Le

Hoang Cac Tien Le is a Master of Engineering student at Ho Chi Minh City University of Technology, Vietnam National University-Ho Chi Minh City, where she also received her BEng in Engineering Physics. Her academic background is rooted in applied physics and engineering, with a primary research focus on the development of advanced biomaterials and their innovative roles in biomedical and technological sectors.

Thi Yen Nhi Nguyen

MEng Thi Yen Nhi Nguyen received her Master of Engineering in Physical Engineering, with a specialization in Biomedical Engineering, from Ho Chi Minh City University of Technology, Vietnam National University Ho Chi Minh City, in 2024. Her research focuses on natural compounds, bioactive substances, and biomedical materials, with an interest in their potential applications in healthcare and therapeutic development.

Vinh-Dat Vuong

Vinh-Dat Vuong is an engineer with ten more years of experience working alongside one of HCMUT's highly efficient research groups. He specializes in materials technology and is responsible for experimental design and data management as well as training other staff in the use of progressive equipment and applications in material synthesis and characterization. Recently, his research focused on electrochemical technologies as well as their applications in pilot production and characterization of nanocomposites.

Open Access Article. Published on 29 April 2026. Downloaded on 6/12/2026 9:42:13 PM. This article is licensed under a Creative Commons Attribution-NonCommercial 3.0 Unported Licence.

hydrogel material formulation suitable for each specific application.[25]

The precise selection and optimization of hydrogel formulations are critical for achieving the desired rheological properties and printability of bioinks. The design of experiments (DoE) methodologies, particularly Box–Behnken design (BBD) and central composite design (CCD),[26] enable simultaneous study of multiple factors,[27] including polymer concentration,[28] cross-linker type, pH, and temperature, to adjust hydrogel properties such as strength, biocompatibility,[29] and viscosity.[30,31] Such multivariate optimization not only elevates reproducibility and bioink performance but also streamlines the synthesis process, reducing time and cost, thereby facilitating the translation of hydrogel-based materials into practical applications in regenerative medicine and tissue engineering.

Complementing DoE strategies, machine learning (ML) has advanced rapidly over the past two decades, demonstrating its capabilities in pattern recognition and parameter optimization across diverse manufacturing processes, including metalworking and additive printing.[32,33] Current applications of ML in 3D bioprinting include optimizing material properties to ensure reliable printability and shape fidelity, regulating the process with the desired fiber and droplet dimensions, and refining structural design to improve cell–microenvironment interactions. Conventional ML models have been applied for prediction, classification, and anomaly detection, underscoring their potential to accelerate design cycles and reproducibility in biofabrication workflows.[34]

In parallel, computational fluid dynamics (CFD) serves as a critical tool for evaluating key parameters in the 3D printing process, including nozzle speed, shear force, printability, and cell viability.[35] CFD simulations enable detailed analysis of fluid flow in the printhead and during bioink deposition, facilitating elucidation of relationships among hydrogel bulk flux, nozzle geometry, shear forces, and print path morphology.[36] CFD applications are not limited to nozzle design but also simulate the interplay between bioink characteristics and nozzle design with cell viability during extrusion.[37] Widely used software platforms such as OpenFOAM, ANSYS Fluent, COMSOL Multiphysics, and FLOW-3D have been used in advancing these simulations.[38,39]

This review provides a comprehensive overview of 3D bioprinting with particular emphasis on hydrogel-based bioinks, including their classification, structures, synthetic strategies, physicochemical properties, and characteristics. Additionally, the integration of DoE, ML, and CFD approaches in the development and optimization of hydrogel systems for bioprinting is critically discussed.

Thi Tan Pham

Associate Professor Thi Tan Pham received his PhD in Physics from Osaka University in 2016 and is currently the Head of the Office of Science and Technology and a faculty member in Biomedical Engineering Physics at Ho Chi Minh City University of Technology, VNU-HCM. His expertise spans optical engineering, nanoarchitectonics, functional nanomaterials, light-emitting devices, graphene-based materials, membranes, and hydrogel materials for 3D-bioink applications. His recent work integrates materials synthesis, response surface methodology, nanostructured platforms, and physicochemical characterization to support reproducible development of advanced biomedical materials.

2. Overview of 3D bioprinting

Traditionally, biological research has been conducted using two-dimensional (2D) rigid platforms such as glass slides, tissue culture plates or animal models. Nonetheless, these methods face many limitations, particularly in accurately replicating and observing physiological characteristics. To enhance the effectiveness of biofabrication techniques, researchers have advanced toward mimicking biological systems through various enabling technologies, with 3D bioprinting emerging as a key approach.[40] This technique is described as ''the application of computer-assisted processes to design and construct living and non-living components in predetermined 2D or 3D configurations, forming engineered biological constructs''.[41]

2.1 Bioinks – hydrogels

Biofabrication is an evolving research discipline focused on generating tissue constructs with hierarchical structural organization. Traditional biofabrication approaches include particulate leaching, lyophilization (freeze-drying), electrospinning, and microfabrication.[42] While each of these methods can produce 3D constructs from a variety of biomaterials, they typically suffer from limited reproducibility and fabrication flexibility. Recently, 3D bioprinting has emerged as an innovative biofabrication technique, significantly enhancing the control and reproducibility of tissue construct fabrication through automated deposition processes.[17,43] In essence, 3D bioprinting enables the production of 3D tissue constructs with predefined architectures and geometries that incorporate biological materials and/or living cells (collectively termed bioinks) by synchronizing the deposition and crosslinking of bioinks with the movement of a mechanical stage.[44] The principal 3D bioprinting modalities include inkjet printing, extrusion-based, and laser-assisted bioprinting,[17] as shown in Fig. 1.

Inkjet bioprinting is a non-contact printing technique capable of depositing bioink in picolitre-scale droplets (1–100 pL) onto substrates with micrometer-scale resolution.[45] During operation, droplets with diameters of approximately 10–50 μm are rapidly generated *via* either thermoelectric or piezoelectric actuation and expelled through a small orifice at the tip of the reservoir.[46,47] In thermal inkjet printing, a heating

© 2026 The Author(s). Published by the Royal Society of Chemistry

Open Access Article. Published on 29 April 2026. Downloaded on 6/12/2026 9:42:13 PM.
This article is licensed under a Creative Commons Attribution-NonCommercial 3.0 Unported Licence.

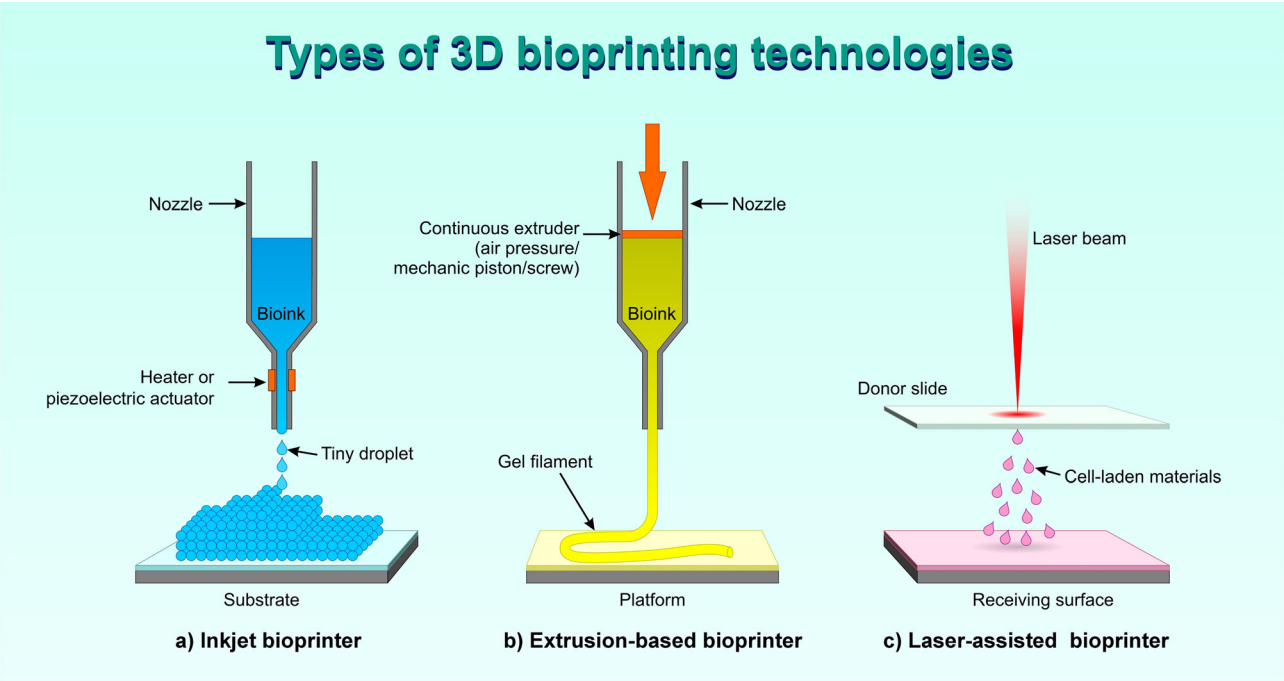

Fig. 1 Types of 3D bioprinting technologies. (a) Inkjet/biodroplet printing. (b) Extrusion-based bioprinting. (c) Laser-assisted bioprinting.

element vaporizes a small volume of bioink inside the reservoir, creating a vapor bubble that propels a droplet through the nozzle. This process briefly exposes encapsulated cells to high temperatures (~300 °C) for a few microseconds (~2 μs), inducing transient pore formation in the cell membrane. By contrast, piezoelectric inkjet systems generate and eject droplets *via* mechanical deformation of a piezoelectric transducer (actuated by an external voltage), thereby avoiding significant temperature increases.[48,49] To prevent nozzle clogging, bioinks used in inkjet printing are formulated with low viscosity (on the order of 1–10 mPa s) and relatively low cell densities (typically below 10^6 cells per mL).[50]

In a typical extrusion-based 3D bioprinting setup, cells suspended in a prepolymer solution are loaded into a syringe or a disposable cartridge and then extruded onto a flat substrate *via* compressed air or mechanical actuation from a rotating piston or screw.[43] Temperature regulation modules are often incorporated into the bioprinter to maintain the bioink at an optimal temperature during printing, which is critical for controlling viscosity and inducing *in situ* solidification.[51] In addition, light sources and specialized nozzle configurations may be integrated to facilitate *in situ* crosslinking of the bioink, thereby enhancing print fidelity and the structural stability of the resulting constructs.[52,53] A major advantage of this approach is its capacity to process highly viscous, high-density bioinks into 3D constructs of clinically relevant size, a capability not achievable with inkjet or laser-assisted bioprinting. Conversely, significant limitations include relatively low resolution (around 200 μm), frequent nozzle clogging, and challenges in fabricating constructs that retain their intended geometry and provide a suitable microenvironment.[43,50] Indeed, fabricating 3D constructs with complex microarchitectures remains a significant challenge in bioprinting. To address these challenges, recent strategies have explored combining multiple crosslinking mechanisms (*e.g.*, photochemical and thermal gelation),[54] and the use of partially crosslinked hydrogels has been investigated with promising results.[49]

Laser-assisted bioprinting utilizes a high-energy pulsed near-infrared laser to irradiate a donor substrate coated with the target bioink, thereby generating a localized jet of droplets. In practice, the laser pulses are focused onto a transparent support (*e.g.*, glass or quartz) coated with a thin metallic layer (commonly gold or titanium) that absorbs the laser energy and transfers it to the bioink. This absorption triggers the rapid formation of a high-pressure vapor bubble, which propels a small bioink droplet toward the receiving substrate.[43,54] Unlike inkjet printing, laser-assisted bioprinting does not suffer from nozzle clogging and can deposit bioinks across a wide viscosity range (1–300 mPa s^{-1}) and at very high cell concentrations (on the order of 10^8 cells per mL).[43] However, achieving high-resolution 3D constructs requires biomaterials that rapidly photo-crosslink upon exposure to the specific laser wavelength, effectively necessitating advanced photo-reactive bioink formulations.[50]

2.2 Factors affecting 3D bioprintability

Printability is an important characteristic of bioinks, as it often decides the extrudability of bioink and the formability of filaments after extrusion.[55] Thus, selecting appropriate bioinks is a critical step in bioprinting processes, particularly with respect to the characteristics of the chosen materials

Open Access Article. Published on 29 April 2026. Downloaded on 6/12/2026 9:42:13 PM. This article is licensed under a Creative Commons Attribution-NonCommercial 3.0 Unported Licence.

(*e.g.*, compatibility with specific printers and achievable resolution) and how these characteristics influence the printing process.[40] Generally, the printability of bioinks is affected by rheological properties, cross-linking mechanisms, and printing conditions.[56]

The rheological characteristics of bioinks, characterized by viscosity, shear stress, viscoelastic shear moduli, and elastic recovery, significantly influence their printability.[57] Recent efforts to optimize bioinks have focused on improving printability and shape accuracy, often through increasing viscosity. However, the ink's bioproperties could be affected, as higher viscosity requires higher extrusion pressure, which can be detrimental to cell viability,[55] and too-viscous bioinks frequently result in poor yield and a non-homogeneous cell distribution.[58] Potent biomaterials should have an adjustable viscosity that can change with temperature and exhibit shear thinning behaviour, as required by different printing methods. Hydrogels exhibiting shear-thinning behaviour are widely regarded as optimal for 3D bioprinting, as they can flow under extrusion and simultaneously protect encapsulated cells from shear stress.[40] Elevating the polymer concentration typically enhances the material's rheological properties. Rheological modifiers such as gelatin or methylcellulose can be incorporated to impart shear-thinning behaviour.[59–61]

The gelation strategy governs compatibility with the selected 3D bioprinting platform, and the gelation duration dictates whether supplementary support structures are required during printing.[40] Mechanisms like photoinitiated crosslinking or thermal gelation stand out as particularly effective options because they can solidify quickly while remaining gentle and cytocompatible, which helps protect encapsulated cells from stress and allows the printed structure to retain its shape right after extrusion.

The inherent biological properties of a bioink formulation play a central role in shaping cellular responses. Important characteristics to evaluate experimentally include the presence of cell adhesive ligands that encourage attachment and the hydrogel matrix's ability to degrade under standard *in vitro* culture conditions. For instance, research has shown that making alginate based bioinks more susceptible to enzymatic degradation leads to markedly improved cell attachment and proliferation throughout the bioprinted construct.[40] These qualities help the material better replicate aspects of the natural extracellular matrix and support more favourable long-term cellular behaviour.

The mechanical properties of bioinks, especially the elastic modulus that reflects stiffness, also have a substantial impact on how cells behave. Differences in modulus can guide important processes such as proliferation, migration, and differentiation by transmitting mechanotransduction signals that cells sense from their surrounding matrix.[40] Carefully tuning these biophysical features therefore becomes essential when designing constructs for biological or tissue engineering purposes.

2.3 Applications

3D bioprinting enables the generation of biological constructs that faithfully replicate native anatomical structures, offering valuable benefits across clinical, research, and educational fields. This approach is widely applied to fabricate cell-laden scaffolds for the regeneration of tissues such as bone, myocardium, cartilage, liver, and lung.

In bone tissue research, 3D bioprinting shows a significant impact on bone treatment and healing by enabling the creation of detailed shapes and greater precision and control over structural components. Gao *et al.* studied the printing of scaffolds using bioinks composed of human mesenchymal stem cells and nanoparticles, such as bioactive glass or hydroxyapatite.[62] Their results indicated that combining hydroxyapatite with the scaffold significantly promoted osteogenic differentiation and osteogenic extracellular matrix production, with a cell viability of 86.62 $\pm$ 6.02%. Besides, the combined scaffolds exhibited a more homogeneous cell distribution, enhanced collagen synthesis, and significantly increased compressive modulus (358.91 $\pm$ 48.05 kPa) after 21 days of culture. A study by Chou *et al.* developed a biodegradable 3D-printed polylactide cage that combines an antibiotic-embedded poly(D,L)-lactide-*co*-glycolide nanofibrous membrane for treating comminuted fractures in rabbit models.[63] The results demonstrated that rabbits receiving the 3D-printed cage implant exhibited improved cortical integrity, leg length ratio, and maximal bending strength.[63] In this study, the 3D-printed PLA cage served as a biodegradable, shape-defined construct capable of capturing comminuted bone fragments, filling the metaphyseal defect, and assisting the intramedullary fixation in maintaining bone length and alignment, whereas the PLGA nanofibrous membrane functioned as the antibiotic-releasing component. This dual-module design differs from conventional hydrogels,[64] which mainly act as resorbable drug depots, and from PMMA cement,[65] which can provide local antibiotic delivery but is non-biodegradable and constrained by heat-related and drug-compatibility limitations. The key contribution of 3D printing is therefore the ability to fabricate a defect-conforming, mechanically supportive, biodegradable cage with controlled architecture, potential extension toward fracture pattern specific or patient matched implants. In cartilage tissue engineering, layered bioprinted scaffolds mimic the native stratified distribution of cells and the extracellular matrix, with precise control over geometry to facilitate chondrocyte differentiation. Incorporation of growth factors, such as TGF-β1 and FGF-2, further enhances glycosaminoglycan production, thereby optimizing the functional properties of the printed cartilage.[66,67]

In the cardiovascular realm, 3D bioprinting has enabled the fabrication of anatomically precise cardiac muscle constructs and heart valve-like structures, which can be further electrically stimulated to restore contractile function. In parallel, coaxial nozzle bioprinting has emerged as a particularly valuable strategy for vascular tissue engineering because it enables the direct fabrication of tubular or core–shell vascular channels through concentric material deposition. In this configuration, the crosslinker flowing through the core stream contacts the hydrogel precursor in the shell stream, leading to rapid *in situ* gelation and immediate formation of hollow tubular

© 2026 The Author(s). Published by the Royal Society of Chemistry

Open Access Article. Published on 29 April 2026. Downloaded on 6/12/2026 9:42:13 PM. This article is licensed under a Creative Commons Attribution-NonCommercial 3.0 Unported Licence.

constructs. This direct core–shell fabrication is difficult to achieve using conventional inkjet or laser-based techniques, which commonly rely on layer-by-layer assembly, scaffold-free spheroid fusion, or fugitive templates to generate perfusable channels after post-print processing. Recent studies further support the unique capability of coaxial bioprinting to produce vascular-like structures with controlled lumen geometry, multimaterial organization, and improved relevance for cardiovascular models, including human coronary artery-sized endothelialized constructs.[68]

For hepatic applications, 3D bioprinting has advanced beyond the simple encapsulation of hepatocytes within bulk hydrogels by enabling the spatially controlled organization of hepatic and non-parenchymal cells into liver-mimetic architectures. Bioinks containing hiPSC-derived hepatocyte-like cells, primary hepatocytes, or hepatocyte-supporting cell co-cultures can be printed into multilayered or lobule-like constructs that partially recapitulate key architectural features of native liver tissue, including defined parenchymal or non-parenchymal cell placement, hexagonal lobule-inspired geometry, and engineered microchannels or sinusoidal-flow environments. Such structural control is important because native liver function depends strongly on microscale organization, heterotypic cell–cell interaction, and mass transport. Original research has shown that rapid 3D bioprinting can pattern hiPSC-derived hepatic progenitor cells together with endothelial and mesenchymal supporting cells in microscale hexagonal units, leading to enhanced hepatic maturation, liver-specific gene expression, metabolic secretion, and cytochrome P450 inducibility.[69] Similarly, 3D bioprinted primary human liver tissues have been used to assess organ-level drug-induced liver injury and to discriminate hepatotoxic responses among clinically relevant compounds.[70] Therefore, the major value of liver bioprinting is not only in providing a permissive hydrogel microenvironment, but also in introducing reproducible, designable tissue architecture that improves physiological relevance for drug metabolism, toxicity screening, disease modelling, and future regenerative applications.

In neural engineering, scaffold free 3D printing of Schwann cells and bone marrow derived stem cells within agarose mold drives self-assembly into nerve grafts, which, upon implantation in animal models, show promise for functional neural regeneration after injury.[71] Building on this foundation, bioprinting is now being applied more broadly in neural engineering to address both peripheral and central nervous system challenges. For peripheral nerve repair, advanced 3D-printed bionic scaffolds loaded with neural crest stem cell-derived Schwann cell progenitors have been developed to guide oriented axonal extension and significantly enhance myelination compared to conventional nerve conduits.[72] Similarly, hydrogel-based constructs containing living Schwann cells printed in aligned architectures maintained high post-printing viability ($>89\%$) and promoted directed neurite outgrowth *in vitro*.[73] In central nervous system applications, 3D bioprinting strategies for spinal cord injury repair have incorporated neural stem cells and glial populations within biomimetic architectures designed to recapitulate native tissue organization and mechanical properties, with several preclinical studies reporting enhanced axonal regeneration and improved functional outcomes.[74]

Skin tissue engineering represents one of the most intensely pursued applications of 3D bioprinting. This technique facilitates the direct deposition of stratified skin layers, including an epidermal layer populated by keratinocytes and a dermal compartment containing fibroblasts within an extracellular matrix. Such bioprinted constructs closely emulate the architecture of native skin, enhancing graft integration and accelerating wound closure. Notably, *in situ* 3D bioprinting whereby skin is printed directly onto the wound bed has demonstrated superior regenerative outcomes compared to conventional dressings and grafting methods.[75] Beyond cutaneous applications, 3D bioprinting has also been extended to pancreatic tissue fabrication: endocrine cell-laden constructs are printed to serve as therapeutic implants for diabetes management; however, optimizing insulin secreting cell function remains challenging due to ionic interactions (*e.g.*, calcium) during crosslinking processes.[76]

Moreover, 3D bioprinting is increasingly leveraged to develop *in vitro* cancer models that faithfully replicate the tumour microenvironment, thereby advancing both basic oncological research and drug development efforts:[77] (i) 3D tumour constructs allow the systematic spatial arrangement of malignant cells alongside stromal and endothelial cell populations, recreating the layered organization of actual tumours. These models enable detailed investigation of cell–cell and cell–matrix interactions, as well as gradients of oxygen, nutrients, and growth factors, offering critical insights into mechanisms of tumour proliferation, invasion, and metastasis. (ii) Bioprinted tumour tissues also serve as high fidelity platforms for anticancer drug screening, improving the predictive accuracy of *in vitro* assays relative to traditional two-dimensional cultures. Consequently, this approach accelerates the identification of promising therapeutic compounds, optimizes dosing regimens, and reduces variability arising from the absence of a realistic tumour microenvironment.

3. Overview of hydrogels

3.1 Definition and classification

Hydrogels are three-dimensional (3D), crosslinked polymeric networks capable of absorbing large amounts of water while maintaining structural integrity, rendering them highly advantageous for biomedical applications, including tissue engineering and 3D bioprinting.[78] Their structural and chemical diversity enables precise tuning of mechanical, rheological, and biological properties, which is critical for advanced biofabrication strategies.[79]

The defining characteristic of hydrogels lies in their crosslinked network architecture, which governs their mechanical strength, swelling behavior, and responsiveness to external stimuli. The classification of hydrogels is shown in Fig. 2. Based

Open Access Article. Published on 29 April 2026. Downloaded on 6/12/2026 9:42:13 PM. This article is licensed under a Creative Commons Attribution-NonCommercial 3.0 Unported Licence.

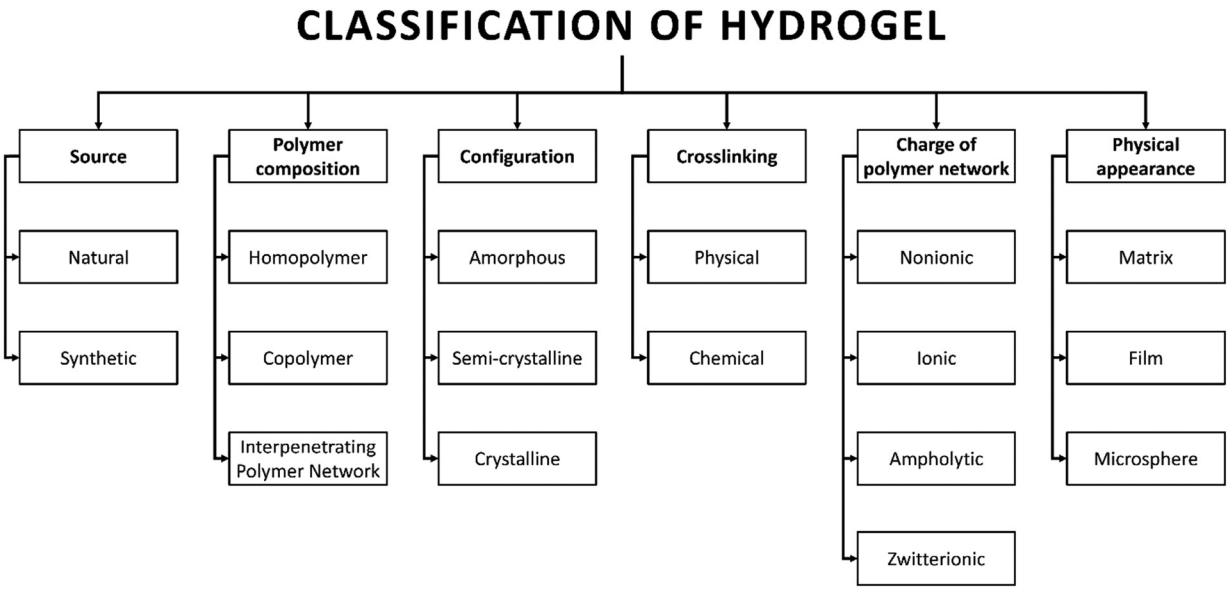

Fig. 2 Classification of hydrogels.

on crosslinking mechanisms, hydrogels are broadly categorized into physically and chemically crosslinked systems.[78] Physically crosslinked hydrogels are formed through reversible non-covalent interactions among polymer chains, including hydrogen bonding,[80,81] ionic interactions,[82] hydrophobic interactions,[83] and other secondary molecular forces.[84] These transient junctions enable dynamic and stimuli-responsive behavior but generally provide lower mechanical robustness compared to covalent networks. In contrast, chemically crosslinked hydrogels rely on permanent covalent bonds to establish stable 3D structures, resulting in improved mechanical integrity and structural resilience. The physical and chemical crosslinking mechanisms in hydrogels are illustrated in Fig. 3. Such networks can be formed through thermal polymerization,[85] photopolymerization,[85–87] enzymatic crosslinking,[88] and other chemical approaches.[89]

Beyond crosslinking type, hydrogel networks exhibit diverse structural organizations that influence functional performance. Based on configuration, hydrogels may be amorphous, semi-crystalline, or crystalline, reflecting differences in structural order and mechanical properties.[79] More advanced architectures include gradient, anisotropic, microstructured, and nanostructured hydrogels. Gradient hydrogels display spatial variations in polymer composition or crosslinking density, often generated *via* controlled mixing of polyethylene glycol (PEG) precursors to create stiffness gradients that guide cellular migration.[90,91] Anisotropic hydrogels exhibit direction-dependent properties achieved through aligned fibers or pores, typically introduced *via* directional freezing or mechanical stretching during gelation.[90] Microstructured hydrogels incorporate micron-scale patterns using techniques such as photolithography on PEG-DA or HEMA precursors,[92] whereas nanostructured hydrogels constructed through nano-molding, initiated chemical vapor deposition, or supramolecular assembly contain nanoscale features such as nanofibers or nanotubes that enhance functionality.[80]

Hydrogels can also be classified according to origin, composition, charge, and morphology. Based on source, they are categorized as natural (*e.g.*, collagen, gelatin, alginate, and chitosan) or synthetic (*e.g.*, polyacrylamide, PEG, and polyvinyl alcohol (PVA)).[93] In terms of polymer composition, hydrogels may be homopolymers, composed of a single repeating monomer unit;[94] copolymers, consisting of multiple monomers arranged in random, block, or alternating sequences;[95] or interpenetrating polymer networks, comprising two entangled networks, including semi-interpenetrating polymer networks with one uncrosslinked polymer for enhanced elasticity and recovery behavior.[96] Network charge further distinguishes hydrogels into nonionic, ionic, ampholytic, and zwitterionic systems, the latter containing both positive and negative charges within each monomer unit.[79] Morphologically, hydrogels may exist in structures as bulk matrices, films, or microspheres, each tailored to specific biomedical applications.[79]

3.2 Characterization of hydrogels

3.2.1 Degree of substitution. The degree of substitution (DoS) quantifies the average number of substituent groups introduced per monomer unit in a polymer chain and is a key parameter in hydrogel synthesis. It reflects the extent of chemical modification and is typically calculated as:[97]

$$\mathrm{DoS}\ (\%) = \left(1 - \frac{\text{apparent sample conc}}{\text{nominal sample conc}}\right) \times 100\%$$

Various techniques can be used to determine DoS, depending on the polymer matrix and substituent groups. The colorimetric method using reagents such as ninhydrin or 2,4,6-trinitrobenzenesulfonic acid is commonly employed to quantify

 © 2026 The Author(s). Published by the Royal Society of Chemistry

Open Access Article. Published on 29 April 2026. Downloaded on 6/12/2026 9:42:13 PM.
This article is licensed under a Creative Commons Attribution-NonCommercial 3.0 Unported Licence.

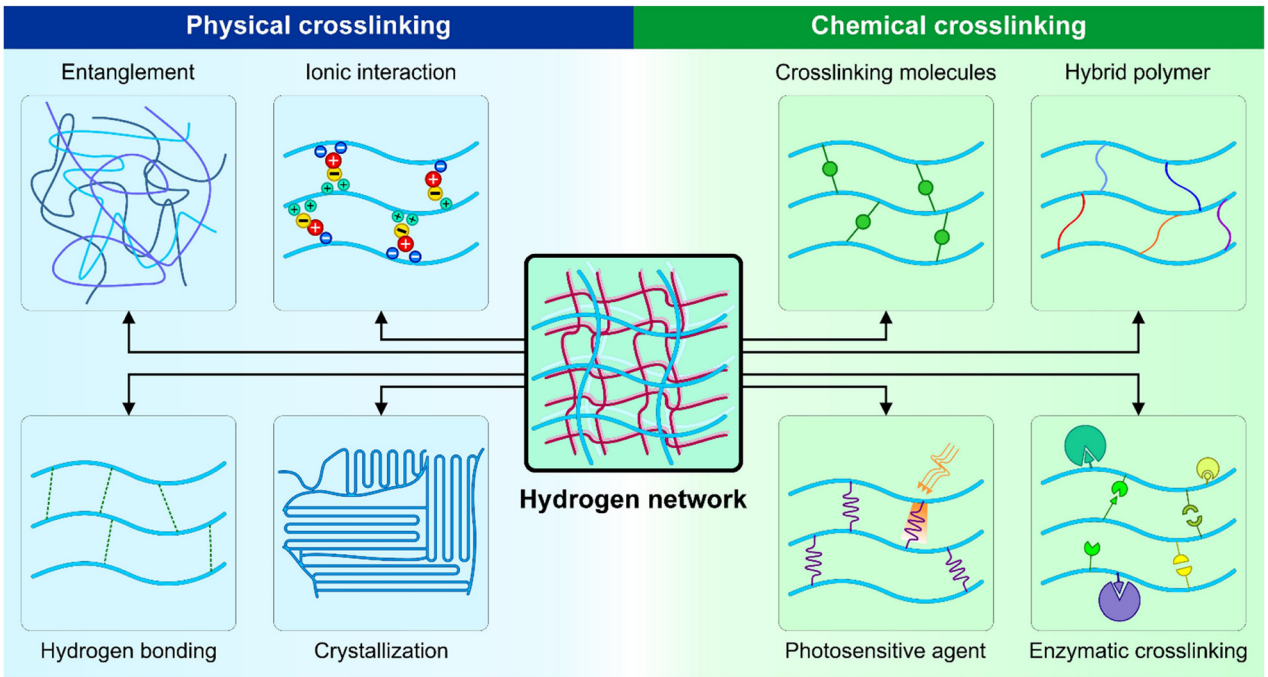

Fig. 3 Diagrammatic representation of the various physical and chemical crosslinking mechanisms in hydrogels.

unreacted amines after reaction with methacryloyl groups in GelMA hydrogels.[98] More precise measurements can be obtained using ^{1}H NMR spectroscopy by integrating characteristic signals of functional groups introduced during modification.[99]

DoS has a significant effect on the physicochemical properties of hydrogels, particularly in 3D bioprinting. An increase in DoS enhances crosslinking density, stiffness, and structural stability, while also reducing swelling capacity.[99–101] Highley *et al.* (2015) demonstrated that tuning DoS enables the fabrication of self-healing, shape-retaining hydrogels.[102]

3.2.2 Morphology. The morphological characteristics of hydrogels, particularly porosity and pore size, are critical for biomedical applications such as tissue engineering and 3D bioprinting. A porous structure not only facilitates water uptake but also promotes cell distribution and tissue ingrowth.[103–105] Pore size greatly affects cellular infiltration and nutrient diffusion, with optimal ranges varying by tissue type: 5–15 μm for fibroblasts, 20–125 μm for skin, and 100–350 μm for bone regeneration.[106]

Hydrogel morphology is commonly characterized by scanning electron microscopy (SEM), following freeze-drying (freeze-drying) to preserve structural integrity. SEM enables high-resolution imaging of hydrogel structures, including pore size, distribution, and network connectivity.[103] Studies using SEM have shown that hydrogels typically exhibit highly porous surfaces with large surface areas, which significantly affect swelling ability and mechanical properties.[107] In addition, SEM is also used to study the effects of environmental factors such as pH and ionic strength on the swelling behaviour of hydrogels, providing important information for tailoring the application of hydrogels in various fields.[103]

Notably, porosity and pore size in hydrogels can be modulated through compositional adjustments. Chen *et al.* reported that the amino group content was inversely proportional to the pore size of GelMA hydrogels.[108] Similarly, Celikkin *et al.* demonstrated that increasing the GelMA concentration reduced both porosity and average pore size.[109] These findings highlight the tunability of hydrogel microstructure, offering strategic opportunities for material optimization in 3D bioprinting.

3.2.3 Mechanical and rheological properties. In 3D bioprinting, the mechanical and rheological properties of hydrogels are critical for ensuring printability, post-printing structural durability, and the ability to support tissue growth. An ideal 3D bioink should exhibit appropriate viscosity, pronounced shear-thinning behaviour, rapid structural recovery, and an optimal crosslinking capacity to maintain its shape after deposition. However, a single universal viscosity value cannot be defined because the printable window depends strongly on the printing modality, nozzle diameter, extrusion pressure, temperature, cell density, and crosslinking mechanism. For extrusion-based bioprinting, which is among the most widely used approaches for hydrogel bioinks, printable materials have been reported across a broad viscosity range of approximately 30 mPa s to 10^{7} mPa s; however, many practical hydrogel inks for direct ink writing or extrusion fall within a low-shear viscosity window of about 10^{2}–10^{6} mPa s.[110] In contrast, inkjet bioprinting generally requires much lower viscosities, commonly below 10–20 mPa s, to enable stable droplet ejection and avoid nozzle clogging.[110]

For extrusion-based printing, shear-thinning behaviour is particularly desirable because the viscosity decreases under high shear inside the nozzle, facilitating smooth extrusion

Open Access Article. Published on 29 April 2026. Downloaded on 6/12/2026 9:42:13 PM. This article is licensed under a Creative Commons Attribution-NonCommercial 3.0 Unported Licence.

and reducing the mechanical stress imposed on encapsulated cells. After deposition, viscosity and elastic recovery should increase rapidly to preserve filament shape and prevent spreading or collapse. This behaviour is commonly described using the power-law or Herschel–Bulkley models, where a flow index (n) < 1 indicates shear-thinning behaviour; values around $n \approx$ 0.3–0.6 are often considered indicative of pronounced shear thinning suitable for smooth extrusion. In addition, a moderate yield stress, typically in the range of 10–1000 Pa, and rapid post-printing recovery, preferably within seconds, are useful design features for maintaining shape fidelity. Therefore, bioink optimization should balance low apparent viscosity during extrusion, sufficient viscosity and elasticity after deposition, and cytocompatible crosslinking to achieve both printability and biological performance.[111]

There are many methods to evaluate the mechanical properties of hydrogels including compression and tension tests to determine the strength and elasticity of the material; dynamic mechanical analysis to test the ability of hydrogels to withstand vibration and deformation; and rheological tests to evaluate the rheological properties and viscosity of hydrogels, which are especially important in 3D printing applications.[112,113]

Rheology describes how hydrogels deform and flow under external forces, reflecting their viscoelastic nature possessing both solid-like and liquid-like behaviour. Key parameters include storage modulus (G'), loss modulus (G''), and loss factor ($\tan\delta$), which are crucial for evaluating printability and structural stability.[114] G' indicates elastic energy storage and mechanical strength, with higher values supporting shape retention after printing. G'' reflects viscous energy dissipation and flowability, facilitating extrusion but potentially compromising shape fidelity. The $\tan\delta$ (G''/G') ratio distinguishes material behaviour: $\tan\delta < 1$ indicates elastic-dominant, while $\tan\delta > 1$ suggests viscous-dominant behaviour.[114,115] The linear viscoelastic region (LVR) defines the strain range where G' and G'' remain stable; printing within this region ensures mechanical integrity and shape recovery.[115]

Cross-linking conditions and polymer composition affect the gelation kinetics and mechanical strength of the hydrogel. Jeong *et al.* reported a temperature-triggered sol–gel transition in chitosan-*graft*-(PEG-PAF), determined by the change in the correlation between G' and G''.[116] Moura *et al.* demonstrated enhanced elastic moduli in genipin-crosslinked chitosan, indicating denser network formation.[117] A physically cross-linked PAA/sodium alginate hydrogel incorporating amorphous calcium carbonate exhibited self-healing behavior and exceptional flexibility, enabling conformation to complex surfaces.[118]

4. Optimization of hydrogel synthesis for 3D bioinks

4.1 Application of DoE in hydrogel synthesis optimization

Traditionally, the development and optimization of biomaterials have relied on one factor-at-a-time approach, which, while widely used[119] is time-consuming, costly, and inadequate for capturing complex factor interactions,[120] resulting in delays in clinical translation.[119] Over the past decade, these traditional methods have been gradually replaced by statistical testing methods such as DoE. DoE enables the simultaneous variation of multiple parameters, thereby increasing experimental efficiency, identifying key contributors to material performance, and supporting predictive model development to streamline optimization.[121,122]

DoE is a statistical method that enables systematic planning and conducting experiments to efficiently extract maximal information from each trial. By elucidating the relationships between independent and dependent variables, DoE facilitates the identification and optimization of critical parameters using a reduced number of experiments.[123,124] To enhance the reliability and objectivity of experimental outcomes, DoE incorporates foundational principles such as replication, randomization, and blocking.[125]

In DoE, response surface methodology (RSM) employs polynomial regression models to investigate the nonlinear effects of multiple factors and determine optimal conditions for the desired response variables.[126–128] Commonly used RSM designs include central composite design (CCD) and Box–Behnken design (BBD), among others.[129,130] Considering specific experimental applications will help clarify the high applicability and optimization efficiency of DoE in hydrogel material research. In practice, DoE has been widely applied to identify and optimize the relationships between input parameters such as polymer concentration, photoinitiator content, environmental conditions or synthesis process parameters with important properties of hydrogels including storage modulus, swelling ratio, rheological behavior, printability, and mechanical strength.[26,131–134] By employing appropriate design models, researchers have not only minimized the number of required experiments but also developed reliable predictive models, thereby guiding the formulation of bioinks tailored to specific requirements in biomedical and tissue engineering applications. Table 1 presents representative studies that have applied various DoE models to optimize hydrogel synthesis, highlighting the role of DoE as a powerful tool for the rational design and development of bioink materials for 3D bioprinting.

The application of response surface methodology in hydrogel optimization has been shown to be effective in improving important properties such as mechanical strength, swelling ability, and rheology. Experimental design models such as CCD, BBD, *etc.* not only reduce the number of experiments required but also provide reliable data to determine the optimal conditions.

4.2 Application of ML in the optimization of hydrogel printability

ML utilizes data-driven statistical relationships to generate predictive models, contrasting with traditional rule-based programming.[135] In 3D bioprinting, ML is increasingly integrated to reduce development time and enhance print fidelity.[32] Although currently in its nascent stages, this integration demonstrates significant potential.[136,137] Key applications

© 2026 The Author(s). Published by the Royal Society of Chemistry

Open Access Article. Published on 29 April 2026. Downloaded on 6/12/2026 9:42:13 PM.
This article is licensed under a Creative Commons Attribution-NonCommercial 3.0 Unported Licence.

Table 1 Summary of DoE applications in optimizing synthesis conditions

Model	Hydrogel	Factor	Response	Results	Ref.
CCD	GelMA/HAMA	Concentrations of GelMA, HAMA, and photoinitiator LAP	Storage modulus and diffusion coefficient	The optimal composition was 8.0% (w/v) GelMA, 2.0% (w/v) HAMA, and 0.1% (w/v) LAP, which achieved a maximum storage modulus of 34.98 kPa and an optimal diffusion coefficient of 1.172×10^{-6} cm^2 s^{-1}, suitable for biomedical applications.	131
	Self-assembling peptide gel (SPG-178)	Peptide (SPG-178) concentration, NaCl concentration, Milieu type	Rheological properties of hydrogels	Helps hydrogels achieve the highest stiffness, suitable for applications in hard tissue and other biomedical fields.	132
	Gum tragacanth-acrylic	pH and concentration of the photoinitiator	Swelling	Helps determine the maximum swelling degree of 5307% when pH $\approx$ 7 and at a photoinitiator concentration of about 21–23 $\times$ 10^{-6} mol L^{-1}	26
BBD	Gel GelMA/HA-Tyr/MC)	GelMA concentration (w/v) HA-Tyr concentration (w/v) Methylcellulose concentration (w/v)	Printability	Helps 3D frames have a stable structure during and after printing, providing greater precision and flexibility	133
Doehlert	GelMA	[MA]/[gelatin] ratio (mL g^{-1}), addition rate of MA (mL min^{-1}), stirring speed (rpm)	Lysine substitution rate, swelling, log G', compressive modulus	– The interaction between temperature and the [MA]/[gelatin] ratio had a positive effect on swelling and a negative effect on log(G') – The interaction between the [MA]/[gelatin] ratio and MA flow rate had a negative effect on lysine substitution rate and compression at 15%	134

include optimizing material properties, tuning printing parameters, enabling *in situ* monitoring, and refining scaffold architectures (Fig. 4).[32]

Traditional ML relies on pre-extracted numerical (*e.g.*, statistical, frequency-domain) or image-based (*e.g.*, edges, textures) features for predictive tasks. Achieving optimal performance necessitates selecting highly relevant and discriminative features.[138] Through iterative training to minimize errors, these models optimize their parameters, enabling them to generalize and accurately predict outcomes for novel inputs.

Depending on the data structure and specific predictive task, these ML models generally utilize three primary approaches: supervised,[139] unsupervised,[140] and reinforcement learning.[141] Supervised learning maps labelled input–output pairs to predict defined outcomes,[139] whereas unsupervised learning extracts intrinsic patterns from unlabelled datasets.[140] Operating between these paradigms, reinforcement learning optimizes actions through evaluative feedback signals rather than relying on explicit target outputs.[141]

Applying these approaches to 3D hydrogel bioprinting, ML not only predicts pre-print material properties but also optimizes process stability and printability. Specifically, it deciphers complex relationships between diverse input parameters (*e.g.*, polymer concentration, printing settings, UV exposure) and critical functional outcomes, such as filament quality, structural integrity, and gelation.[142] Table 2 provides a comprehensive summary of the primary algorithmic categories utilized in hydrogel optimization, highlighting their individual

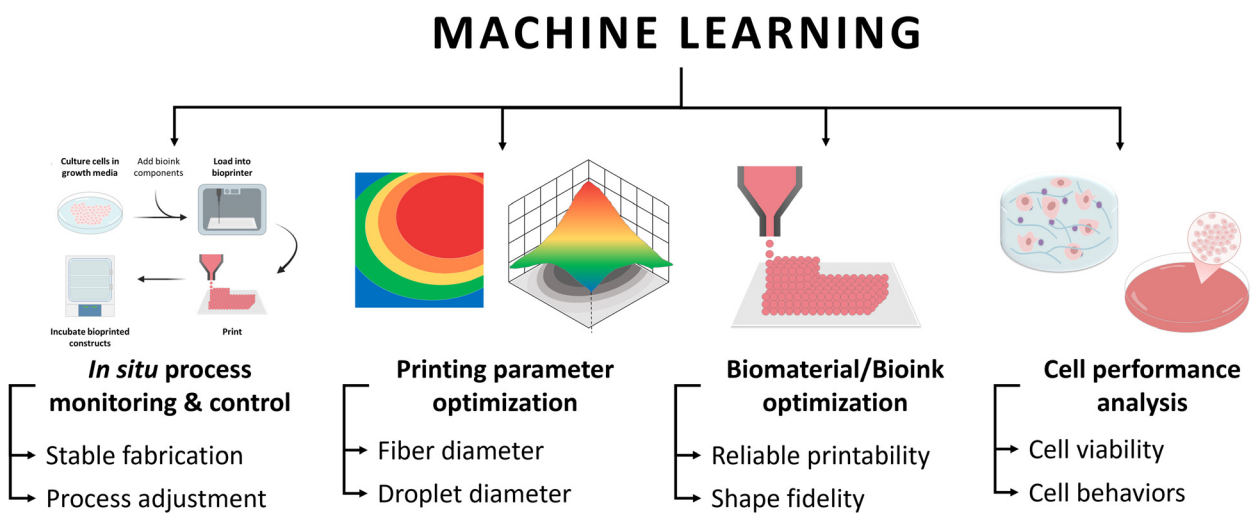

Fig. 4 Applications of machine learning in 3D bioprinting.

Open Access Article. Published on 29 April 2026. Downloaded on 6/12/2026 9:42:13 PM. This article is licensed under a Creative Commons Attribution-NonCommercial 3.0 Unported Licence.

Table 2 Support vector learning algorithms employed for the optimization of hydrogels

Algorithm	Task	Inputs (I)/outputs (O)	Input feature/sample size	Advantages (A)/disadvantages (D)	Ref.
Linear regression	Regression		Input feature: single variable Sample size: small	A: a systematic framework for finding optimal solution paths D: applicable solely to datasets exhibiting linear correlations	146
Multiple linear regression	Prediction of outcomes based on multiple variables	I: printing parameters O: print structure	Input feature: ~3 to 10 variables Sample size: small to medium (20–50 samples)[156,157]	A: fundamental prediction and identification of critical parameters D: this methodology exhibits constraints to improve 3D hydrogel printing because the linearity assumption inadequately represents the nonlinear interactions among factors. The model is also susceptible to noisy data.	143
Decision tree	Classification/regression	I: printing parameters O: classification of target variables or prediction of material properties	Input feature: ~5 to 20 variables Sample size: medium (50–100 samples)[156,158,159]	A: interpretability and the capacity for handling nonlinear interactions D: susceptible to overfitting and sensitive to small alterations	144
Random forest	Classification/regression	I: printing parameters O: prediction of material properties	Input feature: 50 to 100+ variables Sample size: medium to large (>150 samples)[158,159]	A: handling nonlinear interactions D: black-box model with limited interpretability and obscured algorithmic structure	145
LASSO	Feature extraction, regression	I: printing parameters O: important features	Input feature: 10 to 50 initial variables Sample size: small to medium (20–50 samples)[160]	A: feature selection emphasises the identification of variables that have the most major effect on the target variable. D: may overlook interactions due to the assumption of linearity	161
Bayesian optimization	Optimal model design	I: process parameters and feedback O: optimal parameters and prediction plane	Input feature: ~2 to 5 core variables Sample size: very small (<50 iterations)[160,162]	A: performs well with limited data D: exhibits limited generalizability and presents difficulties in scaling	147
Support vector machines	Classification/regression		Input feature: ~5 to 30 variables Sample size: medium (50–100 samples)[156,160]	A: applicable for both classification and regression applications, and capable of integrating Boolean functions B: the system is susceptible to overfitting due to an overwhelming quantity of features, which is accompanied by restricted interpretability of the computational framework.	148

advantages, drawbacks, and applications to clarify the function of various ML methods.

ML utilizes data-driven models to optimize 3D bioprinting, significantly enhancing print fidelity and accelerating development.[32,136,137,143] By extracting discriminative features,[138] ML employs supervised,[139] unsupervised,[140] and reinforcement learning[141] paradigms. In hydrogel bioprinting, these models decipher complex, nonlinear relationships between multivariable inputs (*e.g.*, polymer concentration, UV exposure) and structural outcomes.[142] Specific algorithms address distinct challenges: decision trees and random forests manage nonlinearities and noise,[144,145] multiple linear regression identifies key linear factors,[143,146] Bayesian optimization maximizes limited datasets,[147] and support vector machines balance training efficiency with predictive accuracy.[148,149]

Beyond single algorithms, hybrid ML frameworks significantly enhance predictive performance. For instance, integrating the least absolute shrinkage and selection operator (LASSO) for feature selection with random forests or gradient boosting yields highly accurate models.[150] For global process optimization, Bayesian optimization excels by efficiently identifying near-optimal parameters (*e.g.*, pressure, speed) from limited experimental trials to maximize ''printability scores''.[147,151,152] Table 3 summarizes these diverse ML applications in optimizing hydrogel synthesis and bioprinting workflows. Specific ML models could be applied to address distinct phases of bioprinting. Bayesian optimization rapidly identifies optimal material compositions (*e.g.*, GelMA/HAMA ratios) and printing parameters to maximize printability with minimal experimental expenditure.[147] For natural bioink formulation, integer linear programming combined with multiple regression ensures requisite mechanical properties without chemical modifications.[143] Furthermore, integrating random forests with Boruta (feature selection) and SHAP accurately classifies

 © 2026 The Author(s). Published by the Royal Society of Chemistry

Open Access Article. Published on 29 April 2026. Downloaded on 6/12/2026 9:42:13 PM. This article is licensed under a Creative Commons Attribution-NonCommercial 3.0 Unported Licence.

Table 3 Several ML models are used for synthesis and process optimization in 3D bioprinting of hydrogels

Model	Optimal target	Input	Output	Performance	Ref.
Bayesian optimisation	Evaluate quantitative printability to achieve and accelerate the extrusion printing optimization process	Printing parameters: extrusion pressure, printing speed, temperature and nozzle diameter Composition and concentration of materials (GelMA, HAMA at varying ratios)	Printability score (based on filament formation and layer stacking)	Optimal parameters found with ~19–47 experiments *vs.* ~6000–10 000 possible combinations (*i.e.*, major experiment reduction)	147
Inductive logic programming	Design of bioink from natural materials (collagen, fibrin, hyaluronic acid) for stable 3D printing without chemical modification	Collagen concentration (AC): strongly influences elasticity (G')	Storage modulus (G') for shape fidelity	ML models have successfully identified critical mechanical property windows enabling reliable extrusion and shape fidelity, with experimental confirmation affirming a strong agreement between predicted and measured printability.	143
Multiple regression	Ensure appropriate mechanical properties (elasticity, yield stress) to maintain printed shape	Fibrin concentration: partly determines the yield stress	Yield stress (τ_y) for extrudability		
		Hyaluronic acid concentration (HA): imparts rheological properties (viscosity)	Printability score: determined based on G'–τ_y combination		
Random forest Boruta feature selection SHAP	Identify the key rheological measures that govern the printability of the hydrogel upon the incorporation of rheological additives	A total of 65 initial rheological features derived from frequency sweep, amplitude sweep, and shear-stress-dependent viscosity tests (including G', G'', viscosity, yield stress, damping factor, and flow parameters) across 180 formulations	The 3D printability of each hydrogel was predicted by classifying formulations as ''printable'' or ''not-printable'' based on a printability score threshold of ≥ 0.33.	The model identified 13 critical rheological features strongly associated with printability. Feature reduction improved the $F1$-score for the printable class from 0.91 to 0.94; for the non-printable class, $F1$ = 0.99; OoB score = 0.96, indicating high generalizability and minimal overfitting.	150
Linear regression (LR) Support vector regression Decision tree regression Random forest regression Deep neural network	Predict and optimize the gel fraction of conductive GelMA–PEDOT:SPSS hydrogels to improve curing efficiency and reduce experimental cost	3 feature groups: G1: bioink formulation (GelMA, LAP, PEDOT:SPSS concentration) + UV parameters (intensity, exposure time) G2: absorption coefficient (measured directly using an *in situ* UV sensor during the curing process)	Gel fraction (%)	Best model: SVR (MAPE = 3.13%, R^2 = 0.79) Random forest regression (MAPE = 3.42%, R^2 = 0.76); deep neural network (MAPE = 3.81%, R^2 = 0.74) Absorption coefficient alone: poor performance ($R^2 \leq 0.27$) Combined features improved prediction (best deep neural network: MAPE = 6.31%, R^2 = 0.54)	153
Hierarchical machine learning (HML): Predictor layer → derived physical variable layer → LASSO regression for feature selection and regularization	Identify printing parameters that achieve <10% error in linewidth and corner radius relative to CAD (high-fidelity criterion)	Bottom layer: printing parameters include concentration, nozzle diameter, extrusion speed, and printhead speed. Middle layer: physical variables are calculated from predictors.	Printing fidelity (dimension error in linewidth and corner radius)	R^2 = 0.643 on the test set (HML with middle layer + LASSO leave-one-out CV) Compared to LASSO using only predictors (R^2 = −0.439), the middle layer significantly improves the accuracy of the model.	161

hydrogel printability (out-of-bag score = 0.96) by isolating the 13 most critical rheological features.[150]

Extending ML to crosslinking optimization, support vector regression effectively captures the nonlinear dynamics of GelMA–PEDOT:PSS gelation (MAPE = 3.13%, R^2 = 0.79).[153] Furthermore, hierarchical machine learning (HML) utilizing intermediate physical variables vastly outperforms traditional LASSO (R^2 = 0.643 *vs.* <0).[150] As summarized in Tables 2 and 3, ML offers a scalable toolkit ranging from basic regression to complex ensembles. Moving forward, synergizing these versatile ML algorithms with DoE will be essential to accelerate bioprinting optimization, reduce costs, and ensure structural reproducibility.[119,154,155]

To overcome the resource and cost barriers associated with limited experimental data, optimization strategies utilizing machine learning (ML) algorithms tailored for small datasets

Open Access Article. Published on 29 April 2026. Downloaded on 6/12/2026 9:42:13 PM. This article is licensed under a Creative Commons Attribution-NonCommercial 3.0 Unported Licence.

are proposed. Unlike deep learning models that necessitate vast datasets, Bayesian optimization (BO) enables the identification of optimal printing parameters within merely 19 to 47 experimental iterations.[147] Furthermore, coupling ML with DoE facilitates the generation of highly representative and structured datasets, thereby mitigating the need for large-scale random data collection.[163] Notably, the integration of CFD simulations allows for the prediction of material behavior prior to printing, which significantly reduces the requisite number of physical trials while maintaining high accuracy in capturing complex, nonlinear relationships.[35]

4.3 Applications of CFD in the optimization of hydrogel printability

In the bioprinting field, CFD has become a helpful tool for evaluating key printing parameters, including nozzle velocity, shear stress, printability, and cell viability. Traditionally, optimizing parameters requires multiple experimental iterations, which can significantly increase time and cost to achieve accurate results. Applying CFD simulations can considerably reduce the number of physical experiments required, thereby improving research efficiency.[35] For instance, CFD can be used to simulate the material's flow behaviour and deformation prior to testing to save cost, since the bioinks required for printability testing are often expensive. OpenFOAM software has been applied to examine the relationships among hydrogel flow rate, various nozzle designs, and operating pressure.[36] Similarly, other CFD platforms such as ANSYS Fluent, COMSOL Multiphysics, and FLOW 3D have been utilized to investigate additional design parameters and nozzle configurations. The application of CFD in 3D bioprinting extends beyond nozzle geometry to simulate how bioink characteristics and nozzle design jointly influence cell viability. For instance, COMSOL was used in one study to compare the effect of shear stress on cell viability between cylindrical and conical nozzles.[39]

CFD in hydrogel bioprinting is most impactful when directly linked to experimental bioink behaviour and printing outcomes. Modern CFD studies focus on (i) nozzle geometry optimization to control local shear and extensional flows that determine filament formation and print fidelity; (ii) prediction of shear stresses and residence times that correlate with cell damage or viability; and (iii) process design for high-viscosity dispensing systems (*e.g.*, screw dispensers) and multi-material printheads. These targeted CFD applications have been shown to guide nozzle design parameters (diameter, taper angle, and length), select safe operating windows for extrusion, and reduce the number of empirical trials required for new bioinks.[39,164,165]

CFD methodologies integrate a preprocessor, a flow solver, and a post-processor phase, each facilitated by various software platforms and computational techniques. The general computational workflow is illustrated in Fig. 5, where fluid problems are first formulated based on fluid mechanics principles, translated into the Navier–Stokes equations, discretized using numerical methods, and then solved computationally on structured or unstructured grids to obtain simulation results that are subsequently validated against experimental data. To illustrate the practical implementation of CFD in hydrogel bioprinting, representative simulation platforms and their typical applications are discussed. These tools, such as IPS IBOFlow, COMSOL Multiphysics 4.2, OpenFOAM, and FLOW 3D, have been used to model bioink rheology, nozzle flow behavior, shear-stress distribution, and droplet formation under realistic printing conditions. When employed alongside discrete numerical methods, CFD enables the in-depth assessment of distinct components within diverse bioprinting technologies.[38]

In extrusion-based 3D bioprinting, filament morphology plays a critical role, as it constitutes the foundational elements of printed constructs and directly influences resolution, surface characteristics, and the mechanical stability of the final output. Many studies have been conducted using CFD as a useful tool in the optimization of nozzle design, characterization of bioink rheological behaviour, including flow velocity, pressure gradients, and shear stress, and the evaluation of resultant print attributes such as shape fidelity, biocompatibility, and cell survival rates.[38] CFD simulations have also been effectively employed to predict and optimize printability. By modeling the extrusion process, CFD enables analysis of how flow rate,

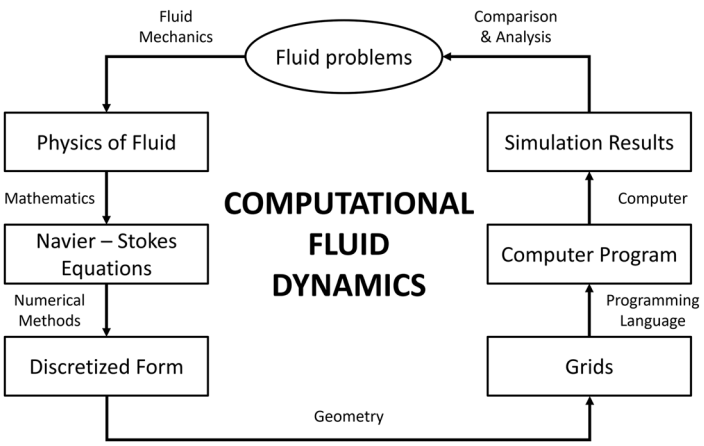

Fig. 5 Computational fluid dynamics process.

 © 2026 The Author(s). Published by the Royal Society of Chemistry

Open Access Article. Published on 29 April 2026. Downloaded on 6/12/2026 9:42:13 PM. This article is licensed under a Creative Commons Attribution-NonCommercial 3.0 Unported Licence.

nozzle geometry, applied pressure, temperature, and ink rheology influence filament formation and diameter.[164] These simulations, as reviewed by Fareez *et al.* (2024), enable computation of relationships between flow parameters, nozzle design, and printing outcomes, and in several studies CFD predictions have been validated experimentally, supporting the use of CFD to guide optimal settings for enhanced print fidelity.[38] A major application of CFD is evaluating bioprinting's impact on cell viability. Wall shear stress within the nozzle is a critical factor influencing cell viability during extrusion-based bioprinting.[38,166] CFD simulations of different nozzle geometries (cylindrical, conical, and tapered) map shear stress fields and correlate them with experimental viability data, revealing a strong inverse relationship between peak shear stress and post-printing cell survival.[35] Conical nozzles produce high but localized shear stress near the tip, while cylindrical nozzles generate lower peak stress over a longer distance, resulting in greater cell damage due to prolonged exposure, insights that guide nozzle redesign to minimize shear while preserving flow.[35] CFD further supports microfluidic integration, where organ-on-a-chip platforms enable precise cell–bioink mixing and multi-material dispensing at micro-scales. By simulating velocity, pressure, and shear rate fields in microchannels, CFD optimizes device design for controlled flow and reduced shear.[167] CFD has been applied to simulate and analyze flow characteristics, including pressure distributions, shear stresses, and oxygen concentration profiles, in perfusable microchannels and engineered tissue constructs. In perfusion models with embedded microchannel networks, CFD enables evaluation of flow velocity, oxygen transport, and shear environments, informing design parameters that improve tissue viability and functional perfusion.[168,169]

Several recent studies exemplify how CFD has been integrated with experiments to address bioprinting-specific questions. Blanco *et al.* review nozzle geometry optimizations that identify favourable internal taper angles and length/diameter ranges to minimize damaging shear while preserving filament continuity; these geometry guidelines have been validated in multiple extrusion experiments.[164] Chand *et al.* and Malekpour *et al.* quantified wall and bulk shear stresses in model bioinks and correlated CFD predicted stress fields with measured cell viability and print quality; these works demonstrate that threshold shear metrics from CFD can be used to screen candidate formulations before wet-lab printing.[35,39] For high viscosity bioinks, Lee *et al.* combined rheological characterization with CFD of a screw based dispenser to predict extrusion pressures and local shear histories, then validated survival and filament fidelity experimentally, which directly reduced the actual iterations required when developing viscous hydrogel inks.[165] Several recent optimization studies demonstrate that surrogate models trained on combined experimental and CFD features improve prediction of printability and cell viability compared with models trained on experimental inputs alone.[170,171] Including CFD features therefore enhances model interpretability by linking physical stresses to outcomes and reduces the need for exhaustive experiments.

5. An integrated DoE–ML–CFD strategy

Optimizing hydrogel bioinks for 3D bioprinting involves navigating a multifaceted design space encompassing material composition, rheological properties, printing parameters, and resulting biological performance (*e.g.*, cell viability and structural fidelity).[172] Traditionally, DoE, ML, and CFD have been used separately to investigate these factors. However, integrating them into a unified DoE–ML–CFD framework enables systematic, efficient improvement of hydrogel performance by combining statistical rigor using DoE, physics-based simulation with CFD, and data-driven prediction through ML, thereby accelerating the discovery of robust bioink formulations.[173,174]

As illustrated in Fig. 6, the refinement cycle requires technically consistent data hand-offs among the DoE, ML, and CFD modules. In the DoE-to-ML transition, experimental outputs such as viscosity, storage or loss moduli, gelation time, extrusion pressure, filament diameter, pore fidelity, and cell viability must be converted into standardized, machine-readable datasets. This step is not trivial because hydrogel datasets are often small, heterogeneous, and sensitive to metadata such as polymer batch, temperature, nozzle diameter, printing pressure, crosslinking method, and measurement shear-rate range. Without consistent units, replicate handling, feature encoding, and uncertainty reporting, ML models may capture experimental artifacts rather than true composition–process–property relationships.

The experimental-to-CFD hand-off is equally important. Rheological data obtained from oscillatory or steady-shear measurements must be translated into constitutive parameters, such as power-law, Herschel–Bulkley, or viscoelastic model coefficients, that can be used as CFD inputs. Errors at this stage can amplify through the entire cycle because an oversimplified viscosity model, an inappropriate shear-rate window, or unrealistic boundary conditions may lead to inaccurate predictions of wall shear stress, pressure drop, residence time, and flow distribution inside the nozzle. Conversely, CFD outputs are usually high-dimensional fields rather than directly usable experimental variables. Therefore, they must be reduced into physically meaningful descriptors, including maximum wall shear stress, average shear exposure, pressure requirement, velocity profile, residence time, and predicted filament expansion, before being integrated into ML models or used to refine the DoE matrix.

In this adaptive cycle, discrepancies among experimental observations, ML predictions, and CFD simulations become decision points for refinement. For example, if ML predicts a formulation to be printable but CFD indicates excessive shear stress that may compromise cell viability, that formulation can be penalized or excluded from the next experimental round. If CFD predicts stable extrusion but the printed filament collapses experimentally, the rheological model, crosslinking kinetics, or boundary conditions must be recalibrated. Similarly, if experimental extrusion pressure or filament morphology deviates from CFD predictions, updated rheological

Open Access Article. Published on 29 April 2026. Downloaded on 6/12/2026 9:42:13 PM.
This article is licensed under a Creative Commons Attribution-NonCommercial 3.0 Unported Licence.

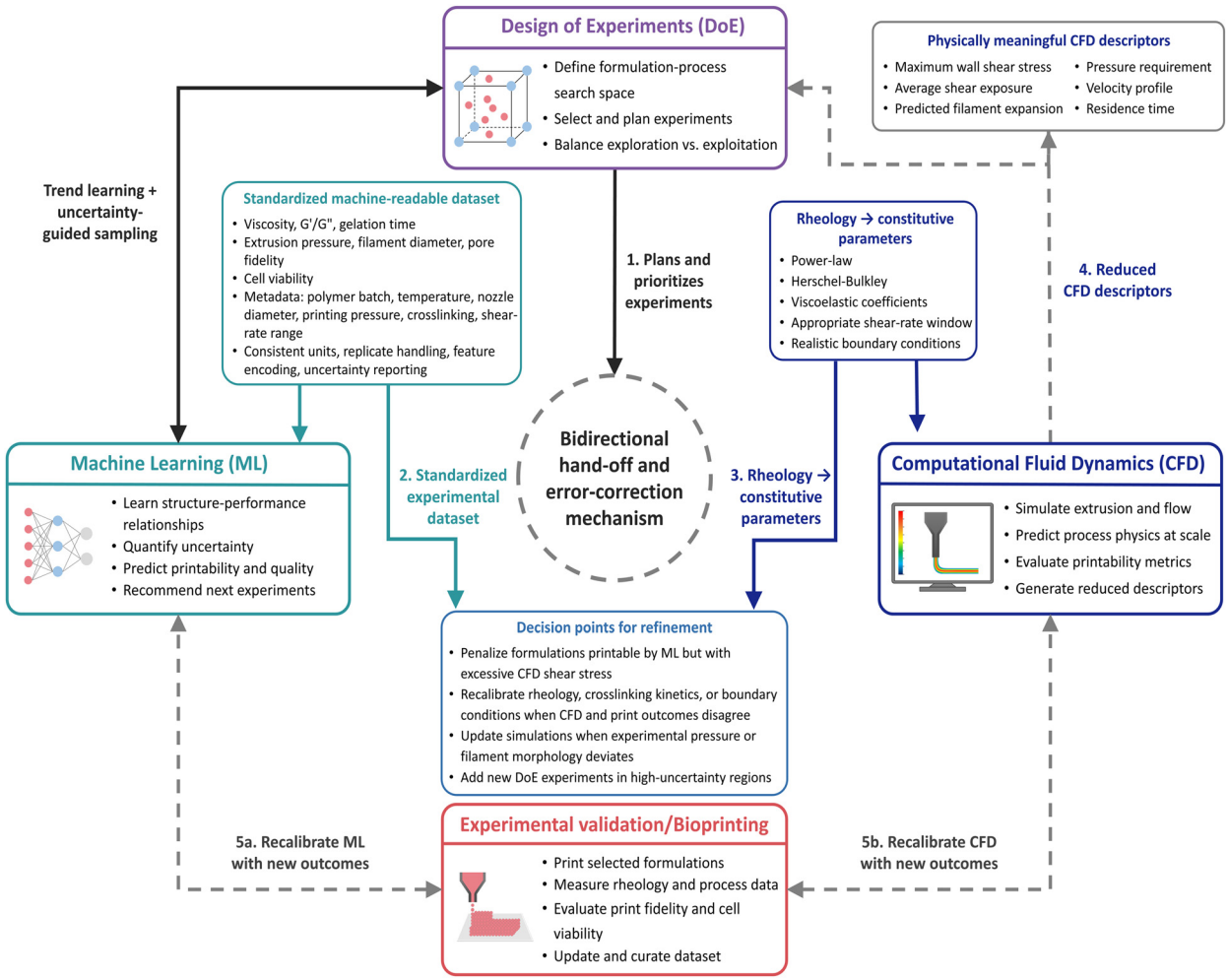

Fig. 6 Integrated DoE–ML–CFD framework for hydrogel bioprinting optimization.

measurements can be fed back into the simulation module. If ML uncertainty is high in a specific formulation region, DoE can prioritize new experiments in that region rather than randomly expanding the dataset. Thus, the dashed arrows in Fig. 6 represent an operational error-correction mechanism: DoE structures the experimental search space, ML identifies nonlinear trends and uncertainty, CFD enforces physical plausibility, and experimental validation recalibrates both models. This bidirectional hand-off transforms the framework into an adaptive optimization cycle that can progressively reduce experimental burden while improving prediction reliability.

Recognizing that multivariable interactions in hydrogel systems are difficult to resolve through conventional trial-and-error approaches, several studies have integrated DoE with ML to construct predictive and statistically structured optimization strategies. For instance, Madadian Bozorg *et al.* employed DoE to vary hydrogel printing parameters and used ML to optimize 3D printing parameters of soft material extrusion, enabling a quality-by-design characterization that systematically explores the effects of key process variables and reduces reliance on traditional trial-and-error approaches.[155] Similarly, Ali Khalvandi *et al.* employed a Box–Behnken DoE to systematically generate porous PVA/gelatin hydrogel formulations and subsequently trained a supervised deep neural network to predict compressive mechanical responses.[163] This approach demonstrated that structured experimental design combined with data-driven modeling can capture nonlinear composition–property relationships and reduce reliance on extensive empirical testing. Such integration enables identification of influential formulation parameters (*e.g.*, the role of crosslinker concentration in modulating viscosity and mechanical properties), thereby supporting rational refinement of bioink formulations toward improved functional performance.[175] Additional studies have combined DoE with supervised ML to predict the compressive behavior of PVA gelatin hydrogels and to guide bioink design as well as structural tuning, including scaffold porosity, in 3D bioprinting workflows.[163,175]

The convergence of ML and CFD is establishing a novel paradigm in 3D bioprinting, facilitating a fundamental shift from empirical, trial-and-error methodologies to quantitative, predictive design strategies.[38,39] In this synergistic framework, CFD functions as a generator of foundational physical data,

© 2026 The Author(s). Published by the Royal Society of Chemistry

Open Access Article. Published on 29 April 2026. Downloaded on 6/12/2026 9:42:13 PM. This article is licensed under a Creative Commons Attribution-NonCommercial 3.0 Unported Licence.

simulating parameters that are experimentally elusive, while ML leverages this dataset to construct high-throughput predictive models for printability and biological functionality.[176,177] A quintessential example of this approach is the work by Zhang *et al.* who successfully established an integrated framework wherein shear stress data derived from CFD simulations were utilized to train a multi-layer perceptron (MLP). This model facilitated the accurate prediction of as-extruded cell viability without necessitating extensive physical experimentation.[173] However, it is critical to acknowledge that the efficacy of this hybrid model is intrinsically linked to the fidelity of CFD input assumptions; inaccuracies in characterizing the viscoelastic properties of bioinks can propagate errors throughout the ML prediction chain.[39,178] Despite these challenges, due to its capacity to significantly abbreviate R&D cycles and optimize resource allocation, the integration of ML and CFD is expected to play an increasingly important role in the fabrication of complex tissue constructs and precision medicine.[179,180]

DoE and CFD bridge experimental efficiency with physical insight: DoE systematically screens influential parameters such as nozzle geometry and material properties, while CFD simulates flow fields and shear stress distributions within the extrusion channel, enabling mechanistic understanding of factors that affect filament formation and cell viability.[172,174] This ensures that simulations are guided by and validated against experimental data.[119] Sun *et al.* demonstrated a synergistic approach combining rheological characterization with CFD simulations to model hydrogel 3D printing behaviour and relate flow properties to printing performance.[181] Chand *et al.* assessed the effects of nozzle geometry and inlet pressure using CFD simulations, quantifying wall shear stress distributions and their potential impact on cell viability.[35] These findings provide mechanistic insights that can inform structured experimental design for extrusion optimization. Concurrently, in the domain of hardware optimization, Reina-Romo *et al.* and Rubio *et al.* pioneered "*in silico*" nozzle design strategies combined with DoE, employing CFD to screen nozzle geometries for minimizing shear-induced cell damage.[164,174] Crucially, CFD does not function as a terminal validation step but as a recalibration mechanism within the loop. Experimental measurements of extrusion pressure or filament morphology can be used to refine rheological inputs and boundary conditions in subsequent simulations. Conversely, CFD-identified stress thresholds can guide the selection of new experimental regions within the DoE matrix. This bidirectional exchange establishes an adaptive cycle in which DoE structures exploration, ML predicts outcomes, and CFD enforces physical plausibility, with each module continuously informing the others rather than operating sequentially.

The selection of optimization strategies in hydrogel-based bioprinting depends on the physicochemical and rheological properties of each material system.[182,183] Fig. 6 illustrates a flexible workflow integrating DoE, ML, and CFD, in which different methods are applied and combined according to the requirements of the hydrogel system. Natural hydrogels, such as collagen, gelatin, and alginate, are widely reported to be biocompatible but mechanically weaker and structurally less defined than synthetic systems, resulting in significant variability and nonlinear structure–property relationships.[182,183] Accordingly, DoE is typically employed to define the formulation-process search space, with key variables including polymer concentration, crosslinker ratio, pH, temperature, and ionic strength, which directly influence viscosity, gelation kinetics, and print fidelity.[184] ML models are then used to capture nonlinear relationships between these variables and performance metrics; for example, elastic modulus and yield stress have been identified as key predictors of printability in ML-assisted bioink design.[142,143] In contrast, synthetic hydrogels, including PEG- and PVA-based systems, exhibit more controlled and reproducible compositions with tuneable physicochemical properties, enabling more systematic parameterization for optimization.[142,182] Within this framework, DoE remains useful for exploring multivariable formulation spaces, particularly for variables such as polymer concentration, initiator content, curing conditions, pH, and temperature, which govern swelling behaviour, porosity, and mechanical strength.[184] ML approaches, including regression-based and tree-based models, have been applied to predict mechanical responses and structure–property relationships in polymer and hydrogel systems under nonlinear or photo-crosslinking conditions.[142] In addition, the relatively well-defined rheological behaviour of synthetic hydrogels allows their description using constitutive models, for example, power-law or Herschel–Bulkley, making them particularly suitable for CFD-based analysis of extrusion dynamics.[181] In such simulations, key parameters include viscosity models, inlet pressure, nozzle geometry, and shear-rate-dependent behaviour, which together determine shear stress distribution, flow stability, and filament formation during printing.[181] For interpenetrating polymer network (IPN) hydrogels, the coexistence of multiple interlaced networks introduces strong coupling between formulation and process variables, leading to highly nonlinear and multiscale behavior.[185] Reviews of IPN systems have shown that while additional networks can enhance mechanical strength and functionality, they also significantly increase the complexity of the design space.[185,186] Consequently, an integrated DoE–ML–CFD strategy is more appropriate for IPN hydrogels, in which DoE defines the multivariable experimental space, ML captures nonlinear interactions and feature importance, and CFD provides physics-based validation of flow and shear conditions.[175] Following optimization, model predictions and simulation outputs are evaluated against experimental observations.[181] If discrepancies arise, the workflow is iteratively redirected to the corresponding module, enabling targeted refinement of the experimental design, retraining of ML models, or recalibration of CFD boundary conditions and constitutive assumptions. This adaptive logic is consistent with recent ML-enabled bioprinting studies that combine experimental datasets with *in silico* predictions to reduce trial-and-error and improve predictive efficiency.[181] In this sense, Fig. 6 captures a modular and iterative optimization framework that integrates experimental design, data-driven modeling, and

Open Access Article. Published on 29 April 2026. Downloaded on 6/12/2026 9:42:13 PM.
This article is licensed under a Creative Commons Attribution-NonCommercial 3.0 Unported Licence.

physics-based simulation into a unified strategy for reproducible hydrogel bioink development.

To make such adaptive cycles reproducible across laboratories, future studies should move toward a standardized bioink metadata schema for FAIR data generation (Fig. 7). At a minimum, this schema should report formulation variables, including polymer type, molecular weight, concentration, degree of substitution, crosslinker or photoinitiator content, pH, ionic strength, pH, and temperature ranges; processing variables, including mixing time, sterilization method, temperature during printing, nozzle diameter, extrusion pressure, printing speed, layer height, and crosslinking dose or duration; and characterization outputs, including viscosity as a function of shear rate, G', G'', $\tan\delta$, yield stress, recovery behaviour, filament diameter, pore fidelity, shape fidelity, and cell viability. For DoE-based studies, the design type, coded and actual factor levels, replicate structure, randomization, response variables, and statistical significance criteria should be explicitly provided. For ML-based studies, dataset size, feature definitions, train/test split, cross-validation strategy, performance metrics such as R^2, RMSE, MAE, accuracy, $F1$-score, or AUC, and uncertainty estimation should be reported. For CFD-assisted studies, the constitutive model, fitted rheological parameters, mesh settings, boundary conditions, convergence criteria, and extracted descriptors such as maximum wall shear stress, pressure drop, residence time, and velocity profile

Fig. 7 Proposed bioink metadata schema for FAIR DoE–ML–CFD workflow.

© 2026 The Author(s). Published by the Royal Society of Chemistry

Open Access Article. Published on 29 April 2026. Downloaded on 6/12/2026 9:42:13 PM. This article is licensed under a Creative Commons Attribution-NonCommercial 3.0 Unported Licence.

should also be included. Such harmonized reporting would make bioink datasets more findable, accessible, interoperable, and reusable, allowing future DoE–ML–CFD workflows to move from isolated case-specific optimization toward cumulative, transferable, and data-driven bioink design.

6. Conclusion

Hydrogel-based bioinks have emerged as promising materials for 3D bioprinting, offering tuneable rheological behaviour, structural fidelity, and biological functionality. While DoE, ML, and CFD have each independently advanced bioink development, their systematic integration into a unified framework represents a critical step toward rational and predictive biofabrication.

The proposed integrated DoE–ML–CFD strategy establishes a structured and adaptive optimization architecture in which statistically designed experiments generate high-quality datasets, ML models capture nonlinear composition–process–property relationships, and CFD simulations provide physics-based validation of extrusion dynamics and shear stress distributions. Through iterative bidirectional refinement, discrepancies between predictions and experimental observations can be progressively minimized, thereby enhancing model robustness and reducing reliance on empirical trial-and-error approaches.

Despite its potential, several challenges remain, including discrepancies between computational predictions and experimental measurements, limited availability of standardized and high-quality bioprinting datasets, and the inherent complexity of cell–material interactions and crosslinking kinetics in biological environments. Addressing these challenges will require improved rheological characterization, standardized reporting practices, and the development of hybrid physics-informed learning models.

Overall, the integration of DoE, ML, and CFD within a closed-loop framework provides a promising pathway toward reproducible, data-driven, and mechanistically informed bioink design, accelerating the translation of 3D bioprinting technologies from experimental research to clinical and industrial applications.

Author contributions

The concepts were proposed by Minh Hien Nguyen and Thi Tan Pham. Minh Hien Nguyen, Gia Huy Duong, Le Thao Vy Huynh, Hoang Cac Tien Le, Thi Yen Nhi Nguyen, Vinh-Dat Vuong and Thi Tan Pham contributed to collecting, summarizing, and evaluating research and news. All authors contributed to drafting and revising the final manuscript.

Conflicts of interest

There are no conflicts to declare.

Data availability

No primary research results, software, or code have been included, and no new data were generated or analysed as part of this review. All information discussed in this article is available in the cited literature.

Acknowledgements

This research was funded by Vietnam National University, Ho Chi Minh City, Vietnam (VNUHCM) under grant number B2025-20-05.

References

1 J. W. Stansbury and M. J. Idacavage, 3D printing with polymers: Challenges among expanding options and opportunities, *Dent. Mater.*, 2016, **32**, 54–64.
2 Wales, International Solid Freeform Fabrication Symposium, 1991, pp. 115–122.
3 B. Khatri, K. Lappe, D. Noetzel, K. Pursche and T. Hanemann, A 3D-Printable Polymer-Metal Soft-Magnetic Functional Composite—Development and Characterization, *Materials*, 2018, **11**, 189.
4 D. Pranzo, P. Larizza, D. Filippini and G. Percoco, Extrusion-Based 3D Printing of Microfluidic Devices for Chemical and Biomedical Applications: A Topical Review, *Micromachines*, 2018, **9**, 374.
5 S. Singh, S. Ramakrishna and R. Singh, Material issues in additive manufacturing: A review, *J. Manuf. Process.*, 2017, **25**, 185–200.
6 A. Arslan-Yildiz, R. El Assal, P. Chen, S. Guven, F. Inci and U. Demirci, Towards artificial tissue models: past, present, and future of 3D bioprinting, *Biofabrication*, 2016, **8**, 14103.
7 A. Munaz, R. K. Vadivelu, J. St. John, M. Barton, H. Kamble and N.-T. Nguyen, Three-dimensional printing of biological matters, *J. Sci.:Adv. Mater. Devices*, 2016, **1**, 1–17.
8 I. T. Ozbolat, Bioprinting scale-up tissue and organ constructs for transplantation, *Trends Biotechnol.*, 2015, **33**, 395–400.
9 J. Zhang, H. Eyisoylu, X.-H. Qin, M. Rubert and R. Müller, 3D bioprinting of graphene oxide-incorporated cell-laden bone mimicking scaffolds for promoting scaffold fidelity, osteogenic differentiation and mineralization, *Acta Biomater.*, 2021, **121**, 637–652.
10 Y. Choi, C. Kim, H. S. Kim, C. Moon and K. Y. Lee, 3D Printing of dynamic tissue scaffold by combining self-healing hydrogel and self-healing ferrogel, *Colloids Surf., B*, 2021, **208**, 112108.
11 S. Ahmed and S. Ikram, Chitosan Based Scaffolds and Their Applications in Wound Healing, *Achiev. Life Sci.*, 2016, **10**, 27–37.
12 M. Abdolahad, H. Taghinejad, A. Saeidi, M. Taghinejad, M. Janmaleki and S. Mohajerzadeh, Cell membrane electrical charge investigations by silicon nanowires

Open Access Article. Published on 29 April 2026. Downloaded on 6/12/2026 9:42:13 PM. This article is licensed under a Creative Commons Attribution-NonCommercial 3.0 Unported Licence.

incorporated field effect transistor (SiNWFET) suitable in cancer research, *RSC Adv.*, 2014, **4**, 7425.
13 C. Mandrycky, Z. Wang, K. Kim and D.-H. Kim, 3D bioprinting for engineering complex tissues, *Biotechnol. Adv.*, 2016, **34**, 422–434.
14 H. J. Lee, Y. B. Kim, S. H. Ahn, J. Lee, C. H. Jang, H. Yoon, W. Chun and G. H. Kim, A New Approach for Fabricating Collagen/ECM-Based Bioinks Using Preosteoblasts and Human Adipose Stem Cells, *Adv. Healthcare Mater.*, 2015, **4**, 1359–1368.
15 C. Benwood, J. Chrenek, R. L. Kirsch, N. Z. Masri, H. Richards, K. Teetzen and S. M. Willerth, Natural Biomaterials and Their Use as Bioinks for Printing Tissues, *Bioengineering*, 2021, **8**, 27.
16 F. L. C. Morgan, L. Moroni and M. B. Baker, Dynamic Bioinks to Advance Bioprinting, *Adv. Healthcare Mater.*, 2020, **9**(15), 1901798.
17 P. S. Gungor-Ozkerim, I. Inci, Y. S. Zhang, A. Khademhosseini and M. R. Dokmeci, Bioinks for 3D bioprinting: an overview, *Biomater. Sci.*, 2018, **6**, 915–946.
18 Z. Xie, M. Gao, A. O. Lobo and T. J. Webster, 3D Bioprinting in Tissue Engineering for Medical Applications: The Classic and the Hybrid, *Polymers*, 2020, **12**, 1717.
19 H. Mao, L. Yang, H. Zhu, L. Wu, P. Ji, J. Yang and Z. Gu, Recent advances and challenges in materials for 3D bioprinting, *Prog. Nat. Sci.:Mater. Int.*, 2020, **30**, 618–634.
20 M. Guvendiren, J. Molde, R. M. D. Soares and J. Kohn, Designing Biomaterials for 3D Printing, *ACS Biomater. Sci. Eng.*, 2016, **2**, 1679–1693.
21 K. Hölzl, S. Lin, L. Tytgat, S. Van Vlierberghe, L. Gu and A. Ovsianikov, Bioink properties before, during and after 3D bioprinting, *Biofabrication*, 2016, **8**, 32002.
22 F.-M. Chen and X. Liu, Advancing biomaterials of human origin for tissue engineering, *Prog. Polym. Sci.*, 2016, **53**, 86–168.
23 B. Liu, J. Li, X. Lei, P. Cheng, Y. Song, Y. Gao, J. Hu, C. Wang, S. Zhang, D. Li, H. Wu, H. Sang, L. Bi and G. Pei, 3D-bioprinted functional and biomimetic hydrogel scaffolds incorporated with nanosilicates to promote bone healing in rat calvarial defect model, *Mater. Sci. Eng., C*, 2020, **112**, 110905.
24 K. C. R. Kolan, J. A. Semon, A. T. Bindbeutel, D. E. Day and M. C. Leu, Bioprinting with bioactive glass loaded polylactic acid composite and human adipose stem cells, *Bioprinting*, 2020, **18**, e00075.
25 E. Aguilar and H. Herrada-Manchón, Editorial for the Special Issue "Hydrogels for 3D Printing", *Gels*, 2024, **10**, 323.
26 B. S. Kaith, R. Sharma, S. Kalia and M. S. Bhatti, Response surface methodology and optimized synthesis of guar gum-based hydrogels with enhanced swelling capacity, *RSC Adv.*, 2014, **4**, 40339–40344.
27 J. Wang, N. Heshmati Aghda, J. Jiang, A. Mridula Habib, D. Ouyang and M. Maniruzzaman, 3D bioprinted microparticles: Optimizing loading efficiency using advanced DoE technique and machine learning modeling, *Int. J. Pharm.*, 2022, **628**, 122302.
28 S. Cardoso, F. Narciso, N. Monge, A. Bettencourt and I. A. C. Ribeiro, Improving Chitosan Hydrogels Printability: A Comprehensive Study on Printing Scaffolds for Customized Drug Delivery, *Int. J. Mol. Sci.*, 2023, **24**, 973.
29 N. V. Arguchinskaya, E. V. Isaeva, A. A. Kisel, E. E. Beketov, T. S. Lagoda, D. S. Baranovskii, N. D. Yakovleva, G. A. Demyashkin, L. N. Komarova, S. O. Astakhina, N. E. Shubin, P. V. Shegay, S. A. Ivanov and A. D. Kaprin, Properties and Printability of the Synthesized Hydrogel Based on GelMA, *Int. J. Mol. Sci.*, 2023, **24**, 2121.
30 N. Rajabi, A. Rezaei, M. Kharaziha, H. R. Bakhsheshi-Rad, H. Luo, S. Ramakrishna and F. Berto, Recent Advances on Bioprinted Gelatin Methacrylate-Based Hydrogels for Tissue Repair, *Tissue Eng., Part A*, 2021, **27**, 679–702.
31 S. Bom, R. Ribeiro, H. M. Ribeiro, C. Santos and J. Marto, On the progress of hydrogel-based 3D printing: Correlating rheological properties with printing behaviour, *Int. J. Pharm.*, 2022, **615**, 121506.
32 J. An, C. K. Chua and V. Mironov, Application of Machine Learning in 3D Bioprinting: Focus on Development of Big Data and Digital Twin, *Int. J. Bioprint.*, 2024, **7**, 342.
33 J. Sun, G. S. Hong, M. Rahman and Y. S. Wong, Improved performance evaluation of tool condition identification by manufacturing loss consideration, *Int. J. Prod. Res.*, 2005, **43**, 1185–1204.
34 J. Sun, K. Yao, K. Huang and D. Huang, Machine learning applications in scaffold based bioprinting, *Mater. Today: Proc.*, 2022, **70**, 17–23.
35 R. Chand, B. S. Muhire and S. Vijayavenkataraman, Computational Fluid Dynamics Assessment of the Effect of Bioprinting Parameters in Extrusion Bioprinting, *Int. J. Bioprint.*, 2022, **8**, 545.
36 J. Leppiniemi, P. Lahtinen, A. Paajanen, R. Mahlberg, S. Metsä-Kortelainen, T. Pinomaa, H. Pajari, I. Vikholm-Lundin, P. Pursula and V. P. Hytönen, 3D-Printable Bioactivated Nanocellulose–Alginate Hydrogels, *ACS Appl. Mater. Interfaces*, 2017, **9**, 21959–21970.
37 H. Ramezani, S. Mohammad Mirjamali and Y. He, Simulations of Extrusion 3D Printing of Chitosan Hydrogels, *Appl. Sci.*, 2022, **12**, 7530.
38 U. N. M. Fareez, S. A. A. Naqvi, M. Mahmud and M. Temirel, Computational Fluid Dynamics (CFD) Analysis of Bioprinting, *Adv. Healthcare Mater.*, 2024, **13**(20), 2400643.
39 A. Malekpour and X. Chen, Printability and Cell Viability in Extrusion-Based Bioprinting from Experimental, Computational, and Machine Learning Views, *J. Funct. Biomater.*, 2022, **13**, 40.
40 A. C. Daly, M. E. Prendergast, A. J. Hughes and J. A. Burdick, Bioprinting for the Biologist, *Cell*, 2021, **184**, 18–32.
41 L. Moroni, J. A. Burdick, C. Highley, S. J. Lee, Y. Morimoto, S. Takeuchi and J. J. Yoo, Biofabrication strategies for 3D in vitro models and regenerative medicine, *Nat. Rev. Mater.*, 2018, **3**, 21–37.
42 P. Bajaj, R. M. Schweller, A. Khademhosseini, J. L. West and R. Bashir, 3D Biofabrication Strategies for Tissue

 © 2026 The Author(s). Published by the Royal Society of Chemistry

Open Access Article. Published on 29 April 2026. Downloaded on 6/12/2026 9:42:13 PM. This article is licensed under a Creative Commons Attribution-NonCommercial 3.0 Unported Licence.

Engineering and Regenerative Medicine, *Annu. Rev. Biomed. Eng.*, 2014, **16**, 247–276.
43 S. V. Murphy and A. Atala, 3D bioprinting of tissues and organs, *Nat. Biotechnol.*, 2014, **32**, 773–785.
44 J. K. Carrow, P. Kerativitayanan, M. K. Jaiswal, G. Lokhande and A. K. Gaharwar, *Polymers for Bioprinting*, Elsevier, 2015, preprint, DOI: 10.1016/B978-0-12-800972-7.00013-X.
45 R. E. Saunders and B. Derby, Inkjet printing biomaterials for tissue engineering: bioprinting, *Int. Mater. Rev.*, 2014, **59**, 430–448.
46 J. Malda, J. Visser, F. P. Melchels, T. Jüngst, W. E. Hennink, W. J. A. Dhert, J. Groll and D. W. Hutmacher, 25th Anniversary Article: Engineering Hydrogels for Biofabrication, *Adv. Mater.*, 2013, **25**, 5011–5028.
47 B. Derby, Inkjet Printing of Functional and Structural Materials: Fluid Property Requirements, Feature Stability, and Resolution, *Annu. Rev. Mater. Res.*, 2010, **40**, 395–414.
48 R. E. Saunders, J. E. Gough and B. Derby, Delivery of human fibroblast cells by piezoelectric drop-on-demand inkjet printing, *Biomaterials*, 2008, **29**, 193–203.
49 R. F. Pereira, A. Sousa, C. C. Barrias, A. Bayat, P. L. Granja and P. J. Bártolo, Advances in bioprinted cell-laden hydrogels for skin tissue engineering, *Biomanuf. Rev.*, 2017, **2**, 1.
50 R. F. Pereira and P. J. Bártolo, 3D bioprinting of photocrosslinkable hydrogel constructs, *J. Appl. Polym. Sci.*, 2015, **132**(48), 42458.
51 F. Guillemot, A. Souquet, S. Catros, B. Guillotin, J. Lopez, M. Faucon, B. Pippenger, R. Bareille, M. Rémy, S. Bellance, P. Chabassier, J. C. Fricain and J. Amédée, High-throughput laser printing of cells and biomaterials for tissue engineering, *Acta Biomater.*, 2010, **6**, 2494–2500.
52 S. Ahn, H. Lee, J. Puetzer, L. J. Bonassar and G. Kim, Fabrication of cell-laden three-dimensional alginate-scaffolds with an aerosol cross-linking process, *J. Mater. Chem.*, 2012, **22**, 18735.
53 L. E. Bertassoni, J. C. Cardoso, V. Manoharan, A. L. Cristino, N. S. Bhise, W. A. Araujo, P. Zorlutuna, N. E. Vrana, A. M. Ghaemmaghami, M. R. Dokmeci and A. Khademhosseini, Direct-write bioprinting of cell-laden methacrylated gelatin hydrogels, *Biofabrication*, 2014, **6**, 24105.
54 S. Wüst, M. E. Godla, R. Müller and S. Hofmann, Tunable hydrogel composite with two-step processing in combination with innovative hardware upgrade for cell-based three-dimensional bioprinting, *Acta Biomater.*, 2014, **10**, 630–640.
55 M. A. Habib and B. Khoda, Rheological analysis of bio-ink for 3D bio-printing processes, *J. Manuf. Process.*, 2022, **76**, 708–718.
56 Z. Zhang, Y. Jin, J. Yin, C. Xu, R. Xiong, K. Christensen, B. R. Ringeisen, D. B. Chrisey and Y. Huang, Evaluation of bioink printability for bioprinting applications, *Appl. Phys. Rev.*, 2018, **5**(4), 041304.
57 D. Venkata Krishna and M. Ravi Sankar, Persuasive factors on the bioink printability and cell viability in the extrusion-based 3D bioprinting for tissue regeneration applications, *Eng. Regener.*, 2023, **4**, 396–410.
58 V. H. M. Mouser, F. P. W. Melchels, J. Visser, W. J. A. Dhert, D. Gawlitta and J. Malda, Yield stress determines bioprintability of hydrogels based on gelatin-methacryloyl and gellan gum for cartilage bioprinting, *Biofabrication*, 2016, **8**, 035003.
59 W. Liu, M. A. Heinrich, Y. Zhou, A. Akpek, N. Hu, X. Liu, X. Guan, Z. Zhong, X. Jin, A. Khademhosseini and Y. S. Zhang, Extrusion Bioprinting of Shear-Thinning Gelatin Methacryloyl Bioinks, *Adv. Healthcare Mater.*, 2017, **6**(10), 1601451.
60 T. Ahlfeld, V. Guduric, S. Duin, A. R. Akkineni, K. Schütz, D. Kilian, J. Emmermacher, N. Cubo-Mateo, S. Dani, M. V. Witzleben, J. Spangenberg, R. Abdelgaber, R. F. Richter, A. Lode and M. Gelinsky, Methylcellulose – a versatile printing material that enables biofabrication of tissue equivalents with high shape fidelity, *Biomater. Sci.*, 2020, **8**, 2102–2110.
61 L. Ouyang, J. P. K. Armstrong, Y. Lin, J. P. Wojciechowski, C. Lee-Reeves, D. Hachim, K. Zhou, J. A. Burdick and M. M. Stevens, Expanding and optimizing 3D bioprinting capabilities using complementary network bioinks, *Sci. Adv.*, 2020, **6**(38), e2205082.
62 G. Gao, A. F. Schilling, T. Yonezawa, J. Wang, G. Dai and X. Cui, Bioactive nanoparticles stimulate bone tissue formation in bioprinted three-dimensional scaffold and human mesenchymal stem cells, *Biotechnol. J.*, 2014, **9**, 1304–1311.
63 Y.-C. Chou, D. Lee, T.-M. Chang, Y.-H. Hsu, Y.-H. Yu, E.-C. Chan and S.-J. Liu, Combination of a biodegradable three-dimensional (3D) – printed cage for mechanical support and nanofibrous membranes for sustainable release of antimicrobial agents for treating the femoral metaphyseal comminuted fracture, *J. Mech. Behav. Biomed. Mater.*, 2017, **72**, 209–218.
64 C. L. Romanò, K. Malizos, N. Capuano, R. Mezzoprete, M. D'Arienzo, C. Van Der, S. Scarponi and L. Drago, Does an Antibiotic-Loaded Hydrogel Coating Reduce Early Post-Surgical Infection After Joint Arthroplasty?, *J. Bone Jt. Infect.*, 2016, **1**, 34–41.
65 S. P. von Hertzberg-Boelch, M. Luedemann, M. Rudert and A. F. Steinert, PMMA Bone Cement: Antibiotic Elution and Mechanical Properties in the Context of Clinical Use, *Biomedicines*, 2022, **10**, 1830.
66 T. Xu, K. W. Binder, M. Z. Albanna, D. Dice, W. Zhao, J. J. Yoo and A. Atala, Hybrid printing of mechanically and biologically improved constructs for cartilage tissue engineering applications, *Biofabrication*, 2012, **5**, 15001.
67 X. Cui, K. Breitenkamp, M. Lotz and D. D'Lima, Synergistic action of fibroblast growth factor-2 and transforming growth factor-beta1 enhances bioprinted human neocartilage formation, *Biotechnol. Bioeng.*, 2012, **109**, 2357–2368.
68 A. Ahmad, S.-J. Kim, Y.-J. Jeong, M. S. Khan, J. Park, D.-W. Lee, C. Lee, Y.-J. Choi and H.-G. Yi, Coaxial bioprinting of a stentable and endothelialized human coronary artery-sized *in vitro* model, *J. Mater. Chem. B*, 2024, **12**, 8633–8646.
69 X. Ma, X. Qu, W. Zhu, Y.-S. Li, S. Yuan, H. Zhang, J. Liu, P. Wang, C. S. E. Lai, F. Zanella, G.-S. Feng, F. Sheikh,

Open Access Article. Published on 29 April 2026. Downloaded on 6/12/2026 9:42:13 PM. This article is licensed under a Creative Commons Attribution-NonCommercial 3.0 Unported Licence.

S. Chien and S. Chen, Deterministically patterned biomimetic human iPSC-derived hepatic model via rapid 3D bioprinting, *Proc. Natl. Acad. Sci. U. S. A.*, 2016, **113**, 2206–2211.

70 D. G. Nguyen, J. Funk, J. B. Robbins, C. Crogan-Grundy, S. C. Presnell, T. Singer and A. B. Roth, Bioprinted 3D Primary Liver Tissues Allow Assessment of Organ-Level Response to Clinical Drug Induced Toxicity In Vitro, *PLoS One*, 2016, **11**, e0158674.

71 A. Faulkner-Jones, C. Fyfe, D.-J. Cornelissen, J. Gardner, J. King, A. Courtney and W. Shu, Bioprinting of human pluripotent stem cells and their directed differentiation into hepatocyte-like cells for the generation of mini-livers in 3D, *Biofabrication*, 2015, **7**, 44102.

72 Y. Li, S. Lv, H. Yuan, G. Ye, W. Mu, Y. Fu, X. Zhang, Z. Feng, Y. He and W. Chen, Peripheral Nerve Regeneration with 3D Printed Bionic Scaffolds Loading Neural Crest Stem Cell Derived Schwann Cell Progenitors, *Adv. Funct. Mater.*, 2021, **31**(16), 2010215.

73 L. Ning, H. Sun, T. Lelong, R. Guilloteau, N. Zhu, D. J. Schreyer and X. Chen, 3D bioprinting of scaffolds with living Schwann cells for potential nerve tissue engineering applications, *Biofabrication*, 2018, **10**, 035014.

74 T. Bedir, S. Ulag, C. B. Ustundag and O. Gunduz, 3D bioprinting applications in neural tissue engineering for spinal cord injury repair, *Mater. Sci. Eng., C*, 2020, **110**, 110741.

75 L. Koch, A. Deiwick, S. Schlie, S. Michael, M. Gruene, V. Coger, D. Zychlinski, A. Schambach, K. Reimers, P. M. Vogt and B. Chichkov, Skin tissue generation by laser cell printing, *Biotechnol. Bioeng.*, 2012, **109**, 1855–1863.

76 I. T. Ozbolat, W. Peng and V. Ozbolat, Application areas of 3D bioprinting, *Drug Discovery Today*, 2016, **21**, 1257–1271.

77 S. Knowlton, S. Onal, C. H. Yu, J. J. Zhao and S. Tasoglu, Bioprinting for cancer research, *Trends Biotechnol.*, 2015, **33**, 504–513.

78 B. S. Kaith, A. Singh, A. K. Sharma and D. Sud, Hydrogels: Synthesis, Classification, Properties and Potential Applications—A Brief Review, *J. Polym. Environ.*, 2021, **29**, 3827–3841.

79 E. M. Ahmed, Hydrogel: Preparation, characterization, and applications: A review, *J. Adv. Res.*, 2015, **6**, 105–121.

80 C. Shao, H. Chang, M. Wang, F. Xu and J. Yang, High-Strength, Tough, and Self-Healing Nanocomposite Physical Hydrogels Based on the Synergistic Effects of Dynamic Hydrogen Bond and Dual Coordination Bonds, *ACS Appl. Mater. Interfaces*, 2017, **9**, 28305–28318.

81 Y. J. Wang, X. N. Zhang, Y. Song, Y. Zhao, L. Chen, F. Su, L. Li, Z. L. Wu and Q. Zheng, Ultrastiff and Tough Supramolecular Hydrogels with a Dense and Robust Hydrogen Bond Network, *Chem. Mater.*, 2019, **31**, 1430–1440.

82 Y. Liang, J. Xue, B. Du and J. Nie, Ultrastiff, Tough, and Healable Ionic–Hydrogen Bond Cross-Linked Hydrogels and Their Uses as Building Blocks To Construct Complex Hydrogel Structures, *ACS Appl. Mater. Interfaces*, 2019, **11**, 5441–5454.

83 Y. Deng, I. Hussain, M. Kang, K. Li, F. Yao, S. Liu and G. Fu, Self-recoverable and mechanical-reinforced hydrogel based on hydrophobic interaction with self-healable and conductive properties, *Chem. Eng. J.*, 2018, **353**, 900–910.

84 C. Löwenberg, M. Balk, C. Wischke, M. Behl and A. Lendlein, Shape-Memory Hydrogels: Evolution of Structural Principles To Enable Shape Switching of Hydrophilic Polymer Networks, *Acc. Chem. Res.*, 2017, **50**, 723–732.

85 H. Wang, D. Zhu, A. Paul, L. Cai, A. Enejder, F. Yang and S. C. Heilshorn, Covalently Adaptable Elastin-Like Protein–Hyaluronic Acid (ELP–HA) Hybrid Hydrogels with Secondary Thermoresponsive Crosslinking for Injectable Stem Cell Delivery, *Adv. Funct. Mater.*, 2017, **27**(28), 1605609.

86 Y. Zhou, K. Liang, S. Zhao, C. Zhang, J. Li, H. Yang, X. Liu, X. Yin, D. Chen, W. Xu and P. Xiao, Photopolymerized maleilated chitosan/methacrylated silk fibroin micro/nanocomposite hydrogels as potential scaffolds for cartilage tissue engineering, *Int. J. Biol. Macromol.*, 2018, **108**, 383–390.

87 T. E. Brown, B. J. Carberry, B. T. Worrell, O. Y. Dudaryeva, M. K. McBride, C. N. Bowman and K. S. Anseth, Photopolymerized dynamic hydrogels with tunable viscoelastic properties through thioester exchange, *Biomaterials*, 2018, **178**, 496–503.

88 Y. Zhou, S. Zhao, C. Zhang, K. Liang, J. Li, H. Yang, S. Gu, Z. Bai, D. Ye and W. Xu, Photopolymerized maleilated chitosan/thiol-terminated poly (vinyl alcohol) hydrogels as potential tissue engineering scaffolds, *Carbohydr. Polym.*, 2018, **184**, 383–389.

89 W. E. Hennink and C. F. van Nostrum, Novel crosslinking methods to design hydrogels, *Adv. Drug Delivery Rev.*, 2012, **64**, 223–236.

90 M. A. Haque, T. Kurokawa and J. P. Gong, Super tough double network hydrogels and their application as biomaterials, *Polymer*, 2012, **53**, 1805–1822.

91 J. A. Burdick, A. Khademhosseini and R. Langer, Fabrication of Gradient Hydrogels Using a Microfluidics/Photopolymerization Process, *Langmuir*, 2004, **20**, 5153–5156.

92 A. Revzin, R. J. Russell, V. K. Yadavalli, W.-G. Koh, C. Deister, D. D. Hile, M. B. Mellott and M. V. Pishko, Fabrication of Poly(ethylene glycol) Hydrogel Microstructures Using Photolithography, *Langmuir*, 2001, **17**, 5440–5447.

93 W. Zhao, X. Jin, Y. Cong, Y. Liu and J. Fu, Degradable natural polymer hydrogels for articular cartilage tissue engineering, *J. Chem. Technol. Biotechnol.*, 2013, **88**, 327–339.

94 T. Iizawa, H. Taketa, M. Maruta, T. Ishido, T. Gotoh and S. Sakohara, Synthesis of porous poly(*N* -isopropylacrylamide) gel beads by sedimentation polymerization and their morphology, *J. Appl. Polym. Sci.*, 2007, **104**, 842–850.

95 L. Yang, J. S. Chu and J. A. Fix, Colon-specific drug delivery: new approaches and in vitro/in vivo evaluation, *Int. J. Pharm.*, 2002, **235**, 1–15.

© 2026 The Author(s). Published by the Royal Society of Chemistry

Open Access Article. Published on 29 April 2026. Downloaded on 6/12/2026 9:42:13 PM. This article is licensed under a Creative Commons Attribution-NonCommercial 3.0 Unported Licence.

96 Z. Maolin, L. Jun, Y. Min and H. Hongfei, The swelling behavior of radiation prepared semi-interpenetrating polymer networks composed of polyNIPAAm and hydrophilic polymers, *Radiat. Phys. Chem.*, 2000, **58**, 397–400.
97 J. M. Zatorski, A. N. Montalbine, J. E. Ortiz-Cárdenas and R. R. Pompano, Quantification of fractional and absolute functionalization of gelatin hydrogels by optimized ninhydrin assay and 1H NMR, *Anal. Bioanal. Chem.*, 2020, **412**, 6211–6220.
98 B. Lee, N. Lum, L. Seow, P. Lim and L. Tan, Synthesis and Characterization of Types A and B Gelatin Methacryloyl for Bioink Applications, *Materials*, 2016, **9**, 797.
99 M. Sun, X. Sun, Z. Wang, S. Guo, G. Yu and H. Yang, Synthesis and Properties of Gelatin Methacryloyl (GelMA) Hydrogels and Their Recent Applications in Load-Bearing Tissue, *Polymers*, 2018, **10**, 1290.
100 B. H. Lee, H. Shirahama, N.-J. Cho and L. P. Tan, Efficient and controllable synthesis of highly substituted gelatin methacrylamide for mechanically stiff hydrogels, *RSC Adv.*, 2015, **5**, 106094–106097.
101 N. Vargas-Alfredo, M. Munar-Bestard, J. M. Ramis and M. Monjo, Synthesis and Modification of Gelatin Methacryloyl (GelMA) with Antibacterial Quaternary Groups and Its Potential for Periodontal Applications, *Gels*, 2022, **8**, 630.
102 C. B. Highley, C. B. Rodell and J. A. Burdick, Direct 3D Printing of Shear-Thinning Hydrogels into Self-Healing Hydrogels, *Adv. Mater.*, 2015, **27**, 5075–5079.
103 M. Azeera, S. Vaidevi and K. Ruckmani, *Characterization Techniques of Hydrogel and Its Applications, in Cellulose-Based Superabsorbent Hydrogels*, Springer, 2019, pp. 737–761.
104 S. Van Vlierberghe, V. Cnudde, P. Dubruel, B. Masschaele, A. Cosijns, I. De Paepe, P. J. S. Jacobs, L. Van Hoorebeke, J. P. Remon and E. Schacht, Porous Gelatin Hydrogels: 1. Cryogenic Formation and Structure Analysis, *Biomacromolecules*, 2007, **8**, 331–337.
105 M. Moazzam, A. Shehzad, D. Sultanova, F. Mukasheva, A. Trifonov, D. Berillo and D. Akilbekova, Macroporous 3D printed structures for regenerative medicine applications, *Bioprinting*, 2022, **28**, e00254.
106 N. Annabi, J. W. Nichol, X. Zhong, C. Ji, S. Koshy, A. Khademhosseini and F. Dehghani, Controlling the Porosity and Microarchitecture of Hydrogels for Tissue Engineering, *Tissue Eng., Part B*, 2010, **16**, 371–383.
107 A. Trifonov, A. Shehzad, F. Mukasheva, M. Moazzam and D. Akilbekova, Reasoning on Pore Terminology in 3D Bioprinting, *Gels*, 2024, **10**, 153.
108 Y. Chen, R. Lin, H. Qi, Y. Yang, H. Bae, J. M. Melero-Martin and A. Khademhosseini, Functional Human Vascular Network Generated in Photocrosslinkable Gelatin Methacrylate Hydrogels, *Adv. Funct. Mater.*, 2012, **22**, 2027–2039.
109 N. Celikkin, S. Mastrogiacomo, J. Jaroszewicz, X. F. Walboomers and W. Swieszkowski, Gelatin methacrylate scaffold for bone tissue engineering: The influence of polymer concentration, *J. Biomed. Mater. Res., Part A*, 2018, **106**, 201–209.
110 A. Schwab, R. Levato, M. D'Este, S. Piluso, D. Eglin and J. Malda, Printability and Shape Fidelity of Bioinks in 3D Bioprinting, *Chem. Rev.*, 2020, **120**, 11028–11055.
111 M. I. Calafel, M. Criado-Gonzalez, R. Aguirresarobe, M. Fernández and C. Mijangos, From rheological concepts to additive manufacturing assessment of hydrogel-based materials for advanced bioprinting applications, *Mater. Adv.*, 2025, **6**, 4566–4597.
112 S. Bashir, Y. Y. Teo, S. Ramesh, K. Ramesh and M. W. Mushtaq, Rheological behavior of biodegradable N-succinyl chitosan-g-poly (acrylic acid) hydrogels and their applications as drug carrier and in vitro theophylline release, *Int. J. Biol. Macromol.*, 2018, **117**, 454–466.
113 M. L. Oyen, Mechanical characterisation of hydrogel materials, *Int. Mater. Rev.*, 2014, **59**, 44–59.
114 H. Herrada-Manchón, M. A. Fernández and E. Aguilar, Essential Guide to Hydrogel Rheology in Extrusion 3D Printing: How to Measure It and Why It Matters?, *Gels*, 2023, **9**, 517.
115 S. Bashir, M. Hina, J. Iqbal, A. H. Rajpar, M. A. Mujtaba, N. A. Alghamdi, S. Wageh, K. Ramesh and S. Ramesh, Fundamental Concepts of Hydrogels: Synthesis, Properties, and Their Applications, *Polymers*, 2020, **12**, 2702.
116 E. Y. Kang, H. J. Moon, M. K. Joo and B. Jeong, Thermogelling Chitosan- *g* -(PAF-PEG) Aqueous Solution As an Injectable Scaffold, *Biomacromolecules*, 2012, **13**, 1750–1757.
117 M. J. Moura, M. M. Figueiredo and M. H. Gil, Rheological Study of Genipin Cross-Linked Chitosan Hydrogels, *Biomacromolecules*, 2007, **8**, 3823–3829.
118 Z. Lei, Q. Wang, S. Sun, W. Zhu and P. Wu, A Bioinspired Mineral Hydrogel as a Self-Healable, Mechanically Adaptable Ionic Skin for Highly Sensitive Pressure Sensing, *Adv. Mater.*, 2017, **29**(22), 1700321.
119 G. Al-Kharusi, N. J. Dunne, S. Little and T. J. Levingstone, The Role of Machine Learning and Design of Experiments in the Advancement of Biomaterial and Tissue Engineering Research, *Bioengineering*, 2022, **9**, 561.
120 M. A. Abdel-Rahman, S. E. D. Hassan, M. N. El-Din, M. S. Azab, E. F. El-Belely, H. M. A. Alrefaey and T. Elsakhawy, One-factor-at-a-time and response surface statistical designs for improved lactic acid production from beet molasses by Enterococcus hirae ds10, *SN Appl. Sci.*, 2020, **2**, 573.
121 A. Dean, D. Voss and D. Draguljić, *Design and Analysis of Experiments*, Springer International Publishing, 2017.
122 S. Zhang, S. Vijayavenkataraman, W. F. Lu and J. Y. H. Fuh, A review on the use of computational methods to characterize, design, and optimize tissue engineering scaffolds, with a potential in 3D printing fabrication, *J. Biomed. Mater. Res., Part B*, 2019, **107**, 1329–1351.
123 R. Potnuri, D. V. Suriapparao, C. S. Rao and T. H. Kumar, Understanding the role of modeling and simulation in pyrolysis of biomass and waste plastics: A review, *Bioresour. Technol. Rep.*, 2022, **20**, 101221.
124 H. M. Kadlimatti, B. Raj Mohan and M. B. Saidutta, Bio-oil from microwave assisted pyrolysis of food

Open Access Article. Published on 29 April 2026. Downloaded on 6/12/2026 9:42:13 PM. This article is licensed under a Creative Commons Attribution-NonCommercial 3.0 Unported Licence.

waste-optimization using response surface methodology, *Biomass Bioenergy*, 2019, **123**, 25–33.
125 P. Sahoo and T. K. Barman, *ANN modelling of fractal dimension in machining*, Elsevier, 2012, preprint, DOI: 10.1533/9780857095893.159.
126 H. Öktem, T. Erzurumlu and H. Kurtaran, Application of response surface methodology in the optimization of cutting conditions for surface roughness, *J. Mater. Process. Technol.*, 2005, **170**, 11–16.
127 M. A. Bezerra, R. E. Santelli, E. P. Oliveira, L. S. Villar and L. A. Escaleira, Response surface methodology (RSM) as a tool for optimization in analytical chemistry, *Talanta*, 2008, **76**, 965–977.
128 S. Santhanam, J. Liang, R. Baid and N. Ravi, Investigating thiol-modification on hyaluronan via carbodiimide chemistry using response surface methodology, *J. Biomed. Mater. Res., Part A*, 2015, **103**, 2300–2308.
129 P. Angelopoulos, H. Evangelaras and C. Koukouvinos, Small, balanced, efficient and near rotatable central composite designs, *J. Stat. Plann. Inference*, 2009, **139**, 2010–2013.
130 S. L. C. Ferreira, R. E. Bruns, H. S. Ferreira, G. D. Matos, J. M. David, G. C. Brandão, E. G. P. da Silva, L. A. Portugal, P. S. dos Reis, A. S. Souza and W. N. L. dos Santos, Box-Behnken design: An alternative for the optimization of analytical methods, *Anal. Chim. Acta*, 2007, **597**, 179–186.
131 A. Talaei, C. D. O'Connell, S. Sayyar, M. Maher, Z. Yue, P. F. Choong and G. G. Wallace, Optimizing the composition of gelatin methacryloyl and hyaluronic acid methacryloyl hydrogels to maximize mechanical and transport properties using response surface methodology, *J. Biomed. Mater. Res., Part B*, 2023, **111**, 526–537.
132 M.-S. Seyedkarimi, H. Mirzadeh, A. Mohammadi and S. Bagheri-Khoulenjani, Mechanical Characteristics of SPG-178 Hydrogels: Optimizing Viscoelastic Properties through Microrheology and Response Surface Methodology, *Iran. Biomed. J.*, 2020, **24**, 110–118.
133 J. Simińska-Stanny, F. Hachemi, G. Dodi, F. D. Cojocaru, I. Gardikiotis, D. Podstawczyk, C. Delporte, G. Jiang, L. Nie and A. Shavandi, Optimizing phenol-modified hyaluronic acid for designing shape-maintaining biofabricated hydrogel scaffolds in soft tissue engineering, *Int. J. Biol. Macromol.*, 2023, **244**, 125201.
134 C. Peyret, K. Elkhoury, S. Bouguet-Bonnet, S. Poinsignon, C. Boulogne, T. Giraud, L. Stefan, Y. Tahri, L. Sanchez-Gonzalez, M. Linder, A. Tamayol, C. J. F. Kahn and E. Arab-Tehrany, Gelatin Methacryloyl (GelMA) Hydrogel Scaffolds: Predicting Physical Properties Using an Experimental Design Approach, *Int. J. Mol. Sci.*, 2023, **24**, 13359.
135 C. Yu and J. Jiang, A Perspective on Using Machine Learning in 3D Bioprinting, *Int. J. Bioprint.*, 2020, **6**, 253.
136 H. Sun, C. P. Kabb, M. B. Sims and B. S. Sumerlin, Architecture-transformable polymers: Reshaping the future of stimuli-responsive polymers, *Prog. Polym. Sci.*, 2019, **89**, 61–75.
137 J. Tan, H. Sun, M. Yu, B. S. Sumerlin and L. Zhang, Photo-PISA: Shedding Light on Polymerization-Induced Self-Assembly, *ACS Macro Lett.*, 2015, **4**, 1249–1253.
138 S. Jie, G. S. Hong, M. Rahman and Y. S. Wong, Feature Extraction and Selection in Tool Condition Monitoring System, in *Proceedings of the International Conference on Artificial Intelligence in Engineering and Technology*, Springer, 2002, pp. 487–497.
139 R. Caruana and A. Niculescu-Mizil, in Proceedings of the 23rd international conference on Machine learning - ICML'06, ACM Press, 2006, pp. 161–168.
140 L. Francis, Unsupervised Learning, in *Predictive Modeling Applications in Actuarial Science*, ed. E. W. Frees, R. A. Derrig and G. Meyers, International Series on Actuarial Science, Cambridge University Press, Cambridge, 2014, pp. 280–312.
141 K. Arulkumaran, M. P. Deisenroth, M. Brundage and A. A. Bharath, Deep Reinforcement Learning: A Brief Survey, *IEEE Signal Process. Mag.*, 2017, **34**, 26–38.
142 J. Shin, Y. Lee, Z. Li, J. Hu, S. S. Park and K. Kim, Optimized 3D Bioprinting Technology Based on Machine Learning: A Review of Recent Trends and Advances, *Micromachines*, 2022, **13**, 363.
143 J. Lee, S. J. Oh, S. H. An, W.-D. Kim and S.-H. Kim, Machine learning-based design strategy for 3D printable bioink: elastic modulus and yield stress determine printability, *Biofabrication*, 2020, **12**, 35018.
144 D. Wu and C. Xu, Predictive Modeling of Droplet Formation Processes in Inkjet-Based Bioprinting, *J. Manuf. Sci. Eng.*, 2018, **140**(10), 101007.
145 H. Xu, Q. Liu, J. Casillas, M. Mcanally, N. Mubtasim, L. S. Gollahon, D. Wu and C. Xu, Prediction of cell viability in dynamic optical projection stereolithography-based bioprinting using machine learning, *J. Intell. Manuf.*, 2022, **33**, 995–1005.
146 G. Shobha and S. Rangaswamy, Machine Learning, 2018, preprint, DOI: 10.1016/bs.host.2018.07.004.
147 K. Ruberu, M. Senadeera, S. Rana, S. Gupta, J. Chung, Z. Yue, S. Venkatesh and G. Wallace, Coupling machine learning with 3D bioprinting to fast track optimisation of extrusion printing, *Appl. Mater. Today*, 2021, **22**, 100914.
148 P. A. Harlianto, T. B. Adji and N. A. Setiawan, in 2017 3rd International Conference on Science and Technology – Computer (ICST), IEEE, 2017, pp. 7–10.
149 J. Kerner, A. Dogan and H. von Recum, Machine learning and big data provide crucial insight for future biomaterials discovery and research, *Acta Biomater.*, 2021, **130**, 54–65.
150 A. Nadernezhad and J. Groll, Machine Learning Reveals a General Understanding of Printability in Formulations Based on Rheology Additives, *Adv. Sci.*, 2022, **9**(29), 2202638.
151 S. Xu, X. Chen, S. Wang, Z. Chen, P. Pan and Q. Huang, Integrating machine learning for the optimization of polyacrylamide/alginate hydrogel, *Regener. Biomater.*, 2024, **11**, rbae109.
152 Y. Xu, R. Sarah, A. Habib, Y. Liu and B. Khoda, Constraint based Bayesian optimization of bioink precursor: a machine learning framework, *Biofabrication*, 2024, **16**, 45031.

© 2026 The Author(s). Published by the Royal Society of Chemistry

Open Access Article. Published on 29 April 2026. Downloaded on 6/12/2026 9:42:13 PM. This article is licensed under a Creative Commons Attribution-NonCommercial 3.0 Unported Licence.

153 X. Huang, Y. X. Wong, G. L. Goh, X. Gao, J. M. Lee and W. Y. Yeong, Machine learning-driven prediction of gel fraction in conductive gelatin methacryloyl hydrogels, *Int. J. AI Mater. Des.*, 2024, **1**, 61.

154 B. MacQueen, R. Jayarathna and J. Lauterbach, Knowledge extraction in catalysis utilizing design of experiments and machine learning, *Curr. Opin. Chem. Eng.*, 2022, **36**, 100781.

155 N. Madadian Bozorg, M. Leclercq, T. Lescot, M. Bazin, N. Gaudreault, A. Dikpati, M.-A. Fortin, A. Droit and N. Bertrand, Design of experiment and machine learning inform on the 3D printing of hydrogels for biomedical applications, *Biomater. Adv.*, 2023, **153**, 213533.

156 M. Li, L. Zhao, Y. Ren, L. Zuo, Z. Shen and J. Wu, The Optimization of Culture Conditions for Injectable Recombinant Collagen Hydrogel Preparation Using Machine Learning, *Gels*, 2025, **11**, 141.

157 S. M. Limon, C. Quigley, R. Sarah and A. Habib, Advancing scaffold porosity through a machine learning framework in extrusion based 3D bioprinting, *Front. Mater.*, 2023, **10**, 1337485.

158 H. Chen, Y. Liu, S. Balabani, R. Hirayama and J. Huang, Machine Learning in Predicting Printable Biomaterial Formulations for Direct Ink Writing, *Research*, 2023, **6**, 0197.

159 R. Sarah, K. Schimmelpfennig, R. Rohauer, C. L. Lewis, S. M. Limon and A. Habib, Characterization and Machine Learning-Driven Property Prediction of a Novel Hybrid Hydrogel Bioink Considering Extrusion-Based 3D Bioprinting, *Gels*, 2025, **11**, 45.

160 J. Sun, K. Yao, J. An, L. Jing, K. Huang and D. Huang, Machine learning and 3D bioprinting, *Int. J. Bioprint.*, 2024, **9**, 717.

161 J. M. Bone, C. M. Childs, A. Menon, B. Póczos, A. W. Feinberg, P. R. LeDuc and N. R. Washburn, Hierarchical Machine Learning for High-Fidelity 3D Printed Biopolymers, *ACS Biomater. Sci. Eng.*, 2020, **6**, 7021–7031.

162 B. Deng, F. L. Lasaosa, D. Chen, C. Zheng, Y. He, C. Xuan, Y. Cui and M. Doblaré, An interactive Bayesian optimization framework for intelligent design of HAMA/GelMA hybrid hydrogels, *Polym. Test.*, 2026, **156**, 109132.

163 A. Khalvandi, L. Tayebi, S. Kamarian, S. Saber-Samandari and J. Song, Data-driven supervised machine learning to predict the compressive response of porous PVA/Gelatin hydrogels and in-vitro assessments: Employing design of experiments, *Int. J. Biol. Macromol.*, 2023, **253**, 126906.

164 J. C. G. Blanco, A. Macías-García, J. M. Rodríguez-Rego, L. Mendoza-Cerezo, F. M. Sánchez-Margallo, A. C. Marcos-Romero and J. B. Pagador-Carrasco, Optimising Bioprinting Nozzles through Computational Modelling and Design of Experiments, *Biomimetics*, 2024, **9**, 460.

165 S. Lee, M. Son, J. Lee, I. Byun, J.-W. Kim, J. Kim and H. Seonwoo, Computational Fluid Dynamics Analysis and Empirical Evaluation of Carboxymethylcellulose/Alginate 3D Bioprinting Inks for Screw-Based Microextrusion, *Polymers*, 2024, **16**, 1137.

166 Q. Liang, Y. Ma, X. Yao and W. Wei, Advanced 3D-Printing Bioinks for Articular Cartilage Repair, *Int. J. Bioprint.*, 2022, **8**, 511.

167 N. R. de Barros, S. V. Harb, C. D. da Silva Horinouchi, L. B. Tofani, D. M. dos Santos, G. B. Elias, J. C. M. Velho, A. C. de Aguiar, M. Sant'Ana and A. C. M. Figueira, Advances in 3D Bioprinting and Microfluidics for Organ-on-a-Chip Platforms, *Polymers*, 2025, **17**, 3078.

168 T. J. Sego, M. Prideaux, J. Sterner, B. P. McCarthy, P. Li, L. F. Bonewald, B. Ekser, A. Tovar and L. Jeshua Smith, Computational fluid dynamic analysis of bioprinted self-supporting perfused tissue models, *Biotechnol. Bioeng.*, 2020, **117**, 798–815.

169 S. Yang, J. Shi, J. Yang, C. Feng and H. Tang, Fluid–Structure Interaction Analysis of Perfusion Process of Vascularized Channels within Hydrogel Matrix Based on Three-Dimensional Printing, *Polymers*, 2020, **12**, 1898.

170 J. Sim and W. K. Chung, Multi-material nozzle geometry design optimization for bioprinting, *Addit. Manuf.*, 2025, **111**, 104959.

171 L. Lemarié, A. Anandan, E. Petiot, C. Marquette and E.-J. Courtial, Rheology, simulation and data analysis toward bioprinting cell viability awareness, *Bioprinting*, 2021, **21**, e00119.

172 J. Karvinen and M. Kellomäki, Design aspects and characterization of hydrogel-based bioinks for extrusion-based bioprinting, *Bioprinting*, 2023, **32**, e00274.

173 C. Zhang, K. C. M. L. Elvitigala, W. Mubarok, Y. Okano and S. Sakai, Machine learning-based prediction and optimisation framework for as-extruded cell viability in extrusion-based 3D bioprinting, *Virtual Phys. Prototyping*, 2024, **19**(1), e2400330.

174 E. Reina-Romo, S. Mandal, P. Amorim, V. Bloemen, E. Ferraris and L. Geris, Towards the Experimentally-Informed In Silico Nozzle Design Optimization for Extrusion-Based Bioprinting of Shear-Thinning Hydrogels, *Front. Bioeng. Biotechnol.*, 2021, **9**, 701778.

175 S. Freeman, S. Calabro, R. Williams, S. Jin and K. Ye, Bioink Formulation and Machine Learning-Empowered Bioprinting Optimization, *Front. Bioeng. Biotechnol.*, 2022, **10**, 913579.

176 S. Ramesh, A. Deep, A. Tamayol, A. Kamaraj, C. Mahajan and S. Madihally, Advancing 3D bioprinting through machine learning and artificial intelligence, *Bioprinting*, 2024, **38**, e00331.

177 S. Tian, R. Stevens, B. McInnes and N. Lewinski, Machine Assisted Experimentation of Extrusion-Based Bioprinting Systems, *Micromachines*, 2021, **12**, 780.

178 G. Ates and P. Bartolo, Computational fluid dynamics for the optimization of internal bioprinting parameters and mixing conditions, *Int. J. Bioprint.*, 2023, **9**, 219.

179 A. Conev, E. E. Litsa, M. R. Perez, M. Diba, A. G. Mikos and L. E. Kavraki, Machine Learning-Guided Three-Dimensional Printing of Tissue Engineering Scaffolds, *Tissue Eng., Part A*, 2020, **26**, 1359–1368.

Open Access Article. Published on 29 April 2026. Downloaded on 6/12/2026 9:42:13 PM.
This article is licensed under a Creative Commons Attribution-NonCommercial 3.0 Unported Licence.

180 A. F. Bonatti, G. Vozzi, C. K. Chua and C. De Maria, A Deep Learning Quality Control Loop of the Extrusion-based Bioprinting Process, *Int. J. Bioprint.*, 2022, **8**, 620.
181 S. Ahmad, H. Alam and P. Thareja, 3D printing of hydrogels: a synergistic approach of rheology and computational fluid dynamics (CFD) modeling, *RSC Adv.*, 2025, **15**, 39369–39390.
182 A. Agrawal and C. M. Hussain, 3D-Printed Hydrogel for Diverse Applications: A Review, *Gels*, 2023, **9**, 960.
183 A. Fatimi, O. V. Okoro, D. Podstawczyk, J. Siminska-Stanny and A. Shavandi, Natural Hydrogel-Based Bio-Inks for 3D Bioprinting in Tissue Engineering: A Review, *Gels*, 2022, **8**, 179.
184 A. Upton, A. Mylona and G. Zimbitas, Utilising design of experiment to design an optimised bioink for 3D bioprinting, *J. Mater. Sci.*, 2025, **60**, 10467–10477.
185 E. S. Dragan, Design and applications of interpenetrating polymer network hydrogels. A review, *Chem. Eng. J.*, 2014, **243**, 572–590.
186 P. A. Panteli and C. S. Patrickios, Multiply Interpenetrating Polymer Networks: Preparation, Mechanical Properties, and Applications, *Gels*, 2019, **5**, 36.

© 2026 The Author(s). Published by the Royal Society of Chemistry